ASN NEURO RESEARCH ARTICLE

ASN NEURO 6(2):art:e00139.doi:10.1042/AN20130044

OPEN ACCESS

Accumulation of amyloid-like $A\beta_{1-42}$ in AEL (autophagy–endosomal–lysosomal) vesicles: potential implications for plaque biogenesis

Daijun Ling*[1], Martha Magallanes* and Paul M. Salvaterra*†[1]

*Department of Neuroscience, Beckman Research Institute of City of Hope, Duarte, CA 91010, U.S.A.

†Irell and Manella Graduate School of Biological Sciences, City of Hope, Duarte, CA 91010, U.S.A.

Cite this article as: Ling D, Magallanes M, Salvaterra PM (2014) Accumulation of amyloid-like $A\beta_{1-42}$ in AEL (autophagy–endosomal–lysosomal) vesicles: potential implications for plaque biogenesis. ASN NEURO 6(2):art:e00139.doi:10.1042/AN20130044

ABSTRACT

Abnormal accumulation of Aβ (amyloid β) within AEL (autophagy–endosomal–lysosomal) vesicles is a prominent neuropathological feature of AD (Alzheimer's disease), but the mechanism of accumulation within vesicles is not clear. We express secretory forms of human $A\beta_{1-40}$ or $A\beta_{1-42}$ in *Drosophila* neurons and observe preferential localization of $A\beta_{1-42}$ within AEL vesicles. In young animals, $A\beta_{1-42}$ appears to associate with plasma membrane, whereas $A\beta_{1-40}$ does not, suggesting that recycling endocytosis may underlie its routing to AEL vesicles. $A\beta_{1-40}$, in contrast, appears to partially localize in extracellular spaces in whole brain and is preferentially secreted by cultured neurons. As animals become older, AEL vesicles become dysfunctional, enlarge and their turnover appears delayed. Genetic inhibition of AEL function results in decreased $A\beta_{1-42}$ accumulation. In samples from older animals, $A\beta_{1-42}$ is broadly distributed within neurons, but only the $A\beta_{1-42}$ within dysfunctional AEL vesicles appears to be in an amyloid-like state. Moreover, the $A\beta_{1-42}$-containing AEL vesicles share properties with AD-like extracellular plaques. They appear to be able to relocate to extracellular spaces either as a consequence of age-dependent neurodegeneration or a non-neurodegenerative separation from host neurons by plasma membrane infolding. We propose that dysfunctional AEL vesicles may thus be the source of amyloid-like plaque accumulation in $A\beta_{1-42}$-expressing *Drosophila* with potential relevance for AD.

Key words: amyloid β, Alzheimer's disease, AEL (autophagy–endosomal–lysosomal) vesicle.

INTRODUCTION

The neuropathology of AD (Alzheimer's disease) is characterized by the accumulation of extracellular amyloid plaques and intracellular neurofibrillary tangles (Perl, 2010). The plaques are composed primarily of $A\beta_{1-42}$ peptide, whereas tangles are composed of hyperphosphorylated tau. The underlying cellular pathogenic mechanisms resulting in these cardinal hallmarks of the disease are not completely understood and even less is known about other types of AD-related neuropathology such as the early intracellular accumulation of GVD (granulovacuolar degeneration) bodies, a feature not only of AD but also other neurodegenerative diseases (Okamoto et al., 1991). GVD bodies exhibit properties of autophagic, endocytic, and lysosomal vesicles (Funk et al., 2011; Ling and Salvaterra, 2011a).

Neurons maintain especially active bidirectional membrane trafficking to and from plasma membrane via recycling endocytosis (Maxfield and McGraw, 2004). Endosomal

[1] Correspondence may be addressed to either of these authors (email psalv@coh.org or lingdaijun@gmail.com).

Abbreviations: Aβ, amyloid β; AD, Alzheimer's disease; AEL, autophagy–endosomal–lysosomal; APP, amyloid precursor protein; CathD, cathepsin D; FA, formic acid; GVD, granulovacuolar degeneration; HRP, horseradish peroxidase; RT–qPCR, reverse transcription–quantitative PCR.

© 2014 The Author(s) This is an Open Access article distributed under the terms of the Creative Commons Attribution Licence (CC-BY) (http://creativecommons.org/licenses/by/3.0/) which permits unrestricted use, distribution and reproduction in any medium, provided the original work is properly cited.

transport vesicles mediate this process, and some ultimately converge by fusion with autophagy and lysosomal vesicles to form AEL (autophagy–endosomal-lysosomal) vesicles (Liou et al., 1997; Saftig and Klumperman, 2009; Manjithaya and Subramani, 2011). Normal AEL vesicle trafficking is essential for intraneuronal signaling, cargo degradation, protein and lipid sorting, axonal transport and synaptic plasticity (Maxfield and McGraw, 2004; Saftig and Klumperman, 2009; Manjithaya and Subramani, 2011) and their abnormal accumulation is one of the earliest events observed in AD pathology (Nixon, 2005; Nixon et al., 2005). Several AEL relevant genes such as *BIN1*, *CD2AP*, *PICALM* and *CD33* are reported to be associated with AD (Hu et al., 2011a, 2011b; Naj et al., 2011). In addition, AEL vesicles have been documented as the main reservoir of intracellular Aβ (amyloid β) peptides, thought to be causative agents of AD pathogenesis (Cataldo et al., 2004; Yu et al., 2005). These Aβ peptides are produced from a sequential proteolysis of APP (amyloid precursor protein) mediated by β- and γ-secretases resulting in Aβ peptides of 39–43 amino acids (the most common AD-associated forms are $A\beta_{1-40}$ and $A\beta_{1-42}$.) Since APP, PS1 (a component of the γ-secretase complex) and BACE1 (the β-secretase) have been localized, at least in part, to AEL vesicles, the vesicles may be a site of amyloidogenic APP processing (Cataldo et al., 2004; Yu et al., 2005). However, this view has been challenged by conflicting observations (Boland et al., 2010) and other studies suggest amyloidogenic APP processing occurs primarily at the plasma membrane (Armstrong, 1998; Takahashi et al., 2002b; Marchesi, 2005). The exact cellular location of Aβ production from APP proteolysis and hence amyloidogenesis is thus still not completely resolved.

In this study, we examine the involvement of the AEL pathway in $A\beta_{1-42}$ accumulation using a well-studied *Drosophila* model of AD (Ling et al., 2009). Direct $A\beta_{1-40}$ or $A\beta_{1-42}$ peptide transgene expression eliminates the need for any APP proteolytic processing, an admittedly different process from that which occurs in AD, but has the advantage of allowing direct observations of peptide routing unconfounded by uncertainties in the various sites proposed for APP proteolysis. The Aβ transgenes we use both contain a secretory signal peptide that directs their initial biosynthesis to the normal cellular secretory pathway, a biosynthetic route shared with APP (Gouras et al., 2005; Laferla et al., 2007). In young flies, $A\beta_{1-42}$ preferentially associates with cellular membranes, especially plasma membranes. Endosomal trafficking may thus account for its specific intracellular accumulation within AEL vesicles relative to $A\beta_{1-40}$. Antibody staining with different aggregation state-specific anti-Aβ antibodies indicates that only $A\beta_{1-42}$ within dysfunctional AEL vesicles in older animals is in an amyloid-like state. The processes of neurodegeneration or non-neurodegenerative plasma membrane infolding may relocalize dysfunctional $A\beta_{1-42}$-containing AEL vesicles to extracellular spaces in older flies, suggesting that this could be the mechanism of plaque formation in *Drosophila*. We present a model for this possibility and discuss its potential relevance for plaque formation in AD.

MATERIALS AND METHODS

Fly strains and Aβ expression

Drosophila melanogaster were raised using standard methods. Human $A\beta_{1-40}$ or $A\beta_{1-42}$ was expressed in *Drosophila* central nervous system using the binary Gal4-UAS technique as illustrated in Supplementary Figures S1A and S1B (at http://www.asnneuro.org/an/006/an006e139add.htm). Fly strains used in this work (including 3.1 kb Gad1-Gal4, 7.4 kb Cha-Gal4, Elav-GeneSwitch-Gal4, UAS-$A\beta_{1-40}$, UAS-$A\beta_{1-42}$, UAS-GFP^{S65T}, UAS-GFP-Atg8a, UAS-$Atg5^{RNAi}$, UAS-$Atg12^{RNAi}$, $Atg1^{\Delta 3D}$) were previously described (Ling et al., 2009; Ling and Salvaterra, 2011b). Additional fly strains are UAS-mCherry-Atg8a (Chang and Neufeld, 2009) and UAS-mRFP-Rab4 (obtained from the Bloomington *Drosophila* Stock Center).

Neuron culture and measurement of Aβ secretion

Embryos at late gastrula stage were collected from Elav-GS-Gal4:UAS-GFP flies that incorporate either the UAS-$A\beta_{1-40}$ or UAS-$A\beta_{1-42}$ transgene. Embryonic cells were dissociated and cultured as described (Salvaterra et al., 1998). Neurons were differentiated for 5 days at 25 °C in Schneider's *Drosophila* medium (Invitrogen) supplemented with 10% FBS, 0.3 μg/ml insulin, 100 U/ml penicillin and 100 μg/ml streptomycin. Culture medium was then replaced by medium with reduced serum (1%) containing 0.1 μM RU486 (Sigma) to induce Aβ expression for 5 days. Parallel cultures with no RU486 inducer served as a negative control. Culture medium was collected for measurement of extracellular Aβ secretion. Cells were harvested and lysed in ice-cold RIPA/SDS buffer [50 mM Tris/HCl (pH 8.0), 0.5% sodium deoxycholate, 1% Triton X-100, 150 mM NaCl and 1% SDS] plus protease inhibitors (Roche). Aβ in culture medium or cell lysate was immunoprecipitated using the anti-Aβ antibody 6E10 (Covance) and Protein A/G plus agarose (Santa Cruz Biotechnology). The immunoprecipitated proteins were eluted and separated by electrophoresis through a 4–20% Tris-glycine gel (Invitrogen), transferred to PVDF membranes and detected using anti-Aβ 6E10 as the primary antibody and HRP (horseradish peroxidase)-conjugated chicken anti-mouse IgG (Santa Cruz Biotechnology) secondary antibody following incubation with SuperSignal West Pico chemiluminescent substrate (Pierce). Densitometric analysis of Western blot bands was performed using ImageJ (NIH). The densitometry of Aβ bands were normalized by the immunoprecipitation antibody bands at 50 kDa (Figures 2C and 2E). For correction of the Aβ species-specific sensitivity to the primary antibody, 1 pmol of synthetic $A\beta_{1-40}$ or $A\beta_{1-42}$ (California Peptide Research) was added to the negative control samples as an Aβ species-specific calibrator.

© 2014 The Author(s) This is an Open Access article distributed under the terms of the Creative Commons Attribution Licence (CC-BY) (http://creativecommons.org/licenses/by/3.0/) which permits unrestricted use, distribution and reproduction in any medium, provided the original work is properly cited.

Cathepsin D activity assay

Frozen heads from 30 adult females were homogenized in 100 μl of ice-cold buffer [10 mM Tris (pH 7.5), 5 mM EDTA and 0.25 M sucrose] and centrifuged at 20 000 ***g*** for 10 min at 4 °C to remove debris, nuclei and large mitochondria. The supernatant was centrifuged at 200 000 ***g*** for 45 min to collect microsomal membranes [i.e. lysosomes, autolysosomes, plasma membranes, ER (endoplasmic reticulum), Golgi, etc.]. The pellet was dissolved in 100 μl of 0.1M sodium acetate buffer (pH 5.0) containing 0.1 % Triton X-100. CathD (cathepsin D) activity was measured as described (Yasuda et al., 1999) using a fluorescently labeled CathD substrate. Samples were incubated at 35 °C in sodium acetate (pH 3.5) for up to 3 h and fluorescence was measured using a SpectraMax microplate reader at 328 nm (excitation) and 393 nm (emission). Enzyme activity was averaged from multiple independently prepared replicates and presented as arbitrary relative fluorescence units/h per μg of protein. Enzyme assays were linear with respect to sample and incubation time. Total proteins were measured using a BCA assay (Pierce) for data normalization.

Western blotting assay

Fly heads from 25-day-old females were homogenized in RIPA/SDS buffer [50 mM Tris/HCl (pH 8.0), 0.5 % sodium deoxycholate, 1 % Triton X-100, 150 mM NaCl and 1 % SDS] with protease inhibitors (Roche Complete). Samples were incubated for 1 h at 4 °C and centrifuged at 12 000 ***g*** for 20 min. The supernatant contained RIPA/SDS-soluble $A\beta_{1-42}$. Pellets were washed with RIPA buffer, homogenized in 70 % FA (formic acid), incubated 1 h at 4 °C and centrifuged at 12 000 ***g*** for 20 min. The supernatant was collected, dried using a SpeedVac centrifuge (Savant) and dissolved in DMSO to obtain FA-soluble $A\beta_{1-42}$. Proteins were separated on 4–20 % polyacrylamide gradient gels (Invitrogen), transferred on to PVDF membranes (Bio-Rad Laboratories), detected by anti-Aβ 6E10 antibody staining (Covance) and HRP-conjugated secondary antibody, and visualized with SuperSignal West Pico chemiluminescent substrate (Pierce) to expose X-ray film. Densitometry of Aβ or loading control bands (40 kDa unspecific protein) was performed using Bio-Rad Quantity-One software.

Immunohistochemistry

Dissected brains were fixed in 4 % paraformaldehyde at 4 °C overnight. For immunostaining using anti-Aβ antibody 4G8 (Covance) or rabbit polyclonal anti-$A\beta_{1-42}$ antibody ab12267 (AbCam), brains were pre-treated with 70 % FA for 10 min. For immunostaining using aggregated-Aβ-specific antibody 7A1a (New England Rare Reagents), FA pre-treatment was not included. Primary antibody immunostaining was detected using Alexa Fluor-555-conjugated secondary antibody (Invitrogen). For immunostaining with anti-Rab5 antibody (AbCam), the secondary antibody used for detection was Alexa Fluor-647-conjugated goat anti-rabbit IgG (Invitrogen). Samples were observed and images collected using confocal microscopy (Zeiss LSM 510).

Congo Red histochemical staining

Fly heads were fixed in 4 % paraformaldehyde at 4 °C for 24 h then washed thoroughly in PBS followed by infiltration with graded concentrations of sucrose. Cryosections were stained with Congo Red (Sigma) following a published procedure (Wilcock et al., 2006). Microscopy images were collected using a 60× objective for both bright-field and dark-field illumination under polarized light.

Fluorescent Congo Red, LysoTracker and CellMask imaging

For Congo Red fluorescence imaging, the brains were fixed and washed as above then stained with 0.2 mg/ml Congo Red in PBS for 10 min. The Congo Red solution was freshly prepared and filtered through a 0.2 μm filter before use. After PBS washing, brains were observed using confocal microscopy. Congo Red fluorescence was detected as described (Wiesehan et al., 2003). LysoTracker red (Molecular Probes) staining was performed as previously described (Ling et al., 2009). For the CellMask plasma membrane staining, whole brains were first immunostained using anti-Aβ 4G8 (Covance) and Alexa Fluor-555-conjugated goat anti-mouse IgG (Invitrogen) secondary antibody, then washed in PBS, followed by a 10 min incubation in PBS containing 5 μg/ml CellMask™ Deep Red plasma membrane stain (Invitrogen). The brains were not permeabilized with detergent prior to the CellMask staining. After 5×PBS washing, brains were mounted and observed by confocal microscopy.

Fluorescence and electron microscopy

Expression of UAS-fluorescent protein transgenes (cytosolic GFP, mCherry-Atg8a, GFP-Atg8a, and mRFP-Rab4) was controlled by a Gal4 driver and fluorescence detected using confocal microscopy on adult brains fixed in PBS with 4 % formaldehyde for 30 min, followed by thorough washing in PBS. Electron microscopy was performed as previously described (Ling et al., 2009) using an FEI Tecnai transmission electron microscope. Independent observations from three to five animals were performed for each experimental condition.

Co-localization analysis

Transgenic GFP-Atg8a and mRFP-Rab4 were expressed in neurons of control, $A\beta_{1-40}$ and $A\beta_{1-42}$ flies. The brains from age-matched female adults were dissected, fixed and observed using confocal microscopy. Kenyon cells from

© 2014 The Author(s) This is an Open Access article distributed under the terms of the Creative Commons Attribution Licence (CC-BY) (http://creativecommons.org/licenses/by/3.0/) which permits unrestricted use, distribution and reproduction in any medium, provided the original work is properly cited.

Drosophila mushroom bodies were selected as the area of interest due to high neuronal density in this brain region. Z-stack images with multiple channels (green for GFP-Atg8a and red for mRFP-Rab4) were collected using a 63× (NA = 1.2) water-immersion objective. At least ten optical sections with z-spacing of 0.5 μm were acquired. Image collection from all samples used identical microscopy conditions including the size of the pinhole, optimized contrast and detector gain. Two independent z-stacks were collected from each brain sample and at least three independent brains were observed for each experimental condition. Co-localization assays were performed using ImageJ (NIH) combined with the Intensity Correlation Analysis plugin (Li et al., 2004). Mander's overlap coefficient was used to quantify co-localization of GFP-Atg8a and mRFP-Rab4 puncta. Mander's overlap coefficient ranges from 0 (no co-localization) to 1 (100% co-localization).

RT–qPCR (reverse transcription–quantitative PCR)

RT-qPCR was performed as described (Ling and Salvaterra, 2011c). The primers for $A\beta_{1-40}$ and $A\beta_{1-42}$ transgenes were 5′-ATGAGTCCAATGATTGCACCT-3′ and 5′-AGACTTTGCATCTGGCTGCTA-3′. Ten reference genes [*14-3-3ε*, *Appl*, *Cyp1*, *Elav*, *eIF-1A*, *l (3)02640*, *Rap2l*, *RpL32*, *Su (Tpl)* and *αTub84B*] were measured for data-specific normalization (Ling and Salvaterra, 2011c). C_T values from real-time PCR were analyzed using a custom SASqPCR program (Ling, 2012). Mean normalized expression ratios were calculated as described (Ling et al., 2012).

Statistical analysis

Image analyses, including densitometric quantification of immunoprecipitation/Western blotting (Figures 2D and 2F), mean signal intensity of anti-Aβ immunostaining (Figure 1C), quantification of the mRFP-Rab4 objects (Figure 5D) and co-localization assay (Figure 5E), were performed using ImageJ (1.45s, NIH). Densitometric analysis of non-immunoprecipitation Western blotting was performed using Bio-Rad Quantity-One (Figure 5). The data analyzer was blinded to image identities relevant to experimental conditions. The sample sizes for biological replicates (n) are provided in relevant Figure legends. Data are presented as means ± S.D. or S.E.M. as indicated. RT–qPCR data analysis for measurement of Aβ transcript levels (Figures 1D and 6D) was as described above. The normalized expression ratios are presented as means ± S.E.M. For all statistical comparisons, two-tailed P values were obtained by Student's t test or ANOVA [corrected for multiple comparisons (Bonferoni) using GraphPad Prism5]. The α-level for all tests was set at 0.05.

RESULTS

$A\beta_{1-42}$ appears to be selectively associated with membrane

Human $A\beta_{1-40}$ or $A\beta_{1-42}$, fused to a rat pre-proenkephalin secretory signal sequence (Finelli et al., 2004), were expressed separately in *Drosophila* neurons using the Gal4:UAS bipartite gene expression technique. Targeted neurons were additionally labeled by co-expression of soluble GFP which initially fills the cytosol and neurites and is detected by fluorescence microscopy (see Supplementary Figure S1). Anti-Aβ antibody 4G8 immunostaining was applied to whole brains to compare the initial accumulation and distribution of $A\beta_{1-40}$ and $A\beta_{1-42}$ peptide in brain region-matched samples from relatively young specimens (1-day-old, relative to eclosion, Figures1A and 1B). The 4G8 antibody targets the 17th–24th amino acids common to both $A\beta_{1-40}$ and $A\beta_{1-42}$. The relative staining intensity appears significantly higher for $A\beta_{1-42}$ than $A\beta_{1-40}$ (Figure 1C). However, transcript levels of $A\beta_{1-42}$ mRNA detected by RT–qPCR are lower than those of $A\beta_{1-40}$ (Figure 1D). The distribution of $A\beta_{1-42}$ staining is strikingly different compared with $A\beta_{1-40}$ staining. $A\beta_{1-42}$ staining appears to outline cell somas (Figure 1B). In brains taken from older specimens (16-day-old) $A\beta_{1-40}$ staining appears to be mostly focal (Figure 1E) and remains less intense than $A\beta_{1-42}$ (Figures 1F and 1G). In these older samples, $A\beta_{1-42}$ staining still appears to be associated with some somal membranes, but staining is also evident in intracellular foci as well as in some likely neurites (Figures 1F and 1G). These intracellular foci were previously identified as dysfunctional autophagy–lysosomal vesicles and their number and size increases with age specifically in $A\beta_{1-42}$-expressing samples (Ling et al., 2009). Our results suggest that $A\beta_{1-42}$ may preferentially associate with various membranous structures, including plasma membranes, whereas $A\beta_{1-40}$ does not.

Neurons preferentially secrete $A\beta_{1-40}$ but retain $A\beta_{1-42}$

The C-terminus of $A\beta_{1-42}$ has an additional isoleucine and alanine relative to $A\beta_{1-40}$ that increases its hydrophobicity and membrane association (Marchesi, 2005). This increased membrane association may contribute to its greater accumulation within neurons by interfering with efficient secretion following biosynthesis through the secretory pathway. To obtain evidence for this possibility, we double-stained fly brains expressing Aβ with anti-Aβ 4G8 antibody and CellMask, a plasma membrane-specific fluorescent dye. In 1-day-old $A\beta_{1-42}$ samples we observe extensive co-localization of antibody staining with CellMask staining (Figure 2B) suggesting an association of $A\beta_{1-42}$ with plasma membranes. In contrast, $A\beta_{1-40}$ samples exhibit only limited co-localization of a few plasma membrane foci along with some intracellular

© 2014 The Author(s) This is an Open Access article distributed under the terms of the Creative Commons Attribution Licence (CC-BY) (http://creativecommons.org/licenses/by/3.0/) which permits unrestricted use, distribution and reproduction in any medium, provided the original work is properly cited.

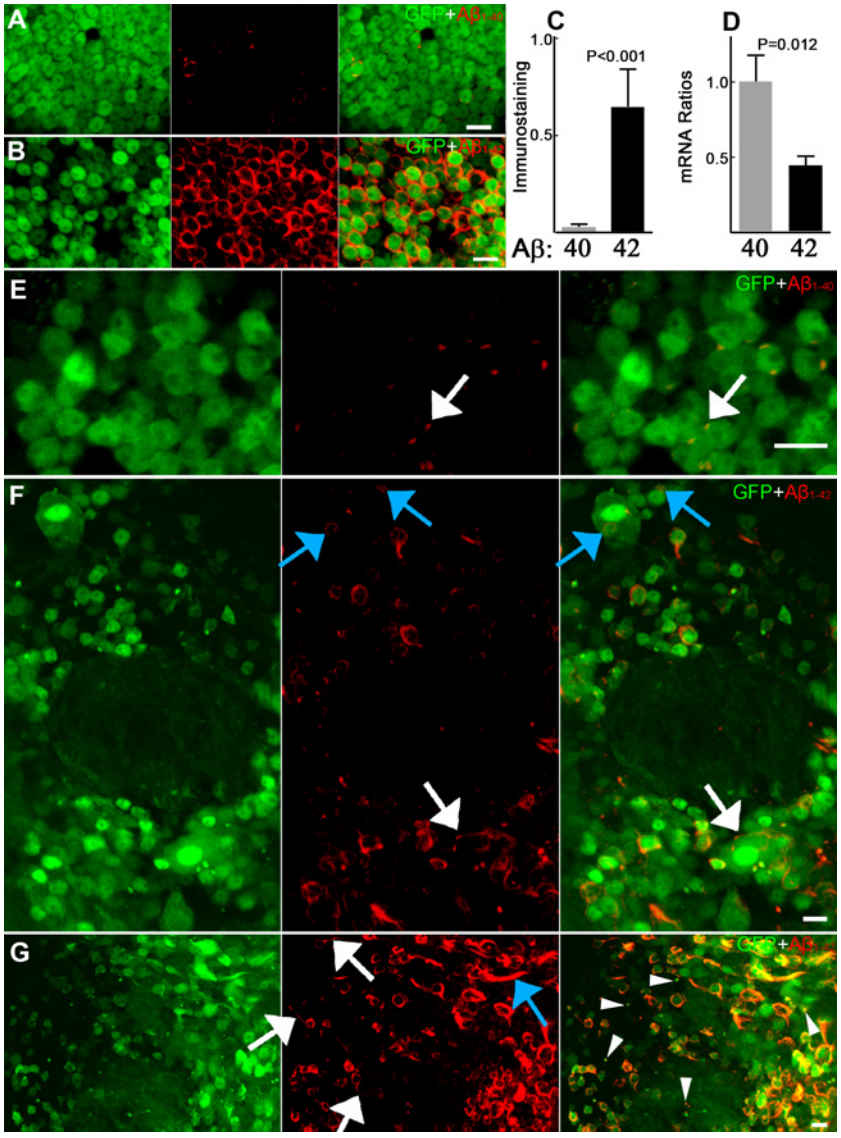

Figure 1 **Differential accumulation of $A\beta_{1-40}$ and $A\beta_{1-42}$**

(**A**, **B**) Anti-Aβ 4G8 immunostaining of whole fly brains expressing either $A\beta_{1-40}$ (**A**) or $A\beta_{1-42}$ (**B**) at age of 1 day. (**C**) Quantification of the immunostaining signals for $A\beta_{1-40}$ ($n = 3$) and $A\beta_{1-42}$ ($n = 5$). The mean intensity of anti-Aβ immunostaining signals were normalized to the mean intensity of GFP signal. Data represent means ± S.D. (**D**) RT–qPCR detection of Aβ transcript levels of $A\beta_{1-40}$ or $A\beta_{1-42}$ transgene expression in fly heads. Data represent means ± S.E.M. (**E**–**G**) Anti-Aβ 4G8 immunostaining shows the distribution of $A\beta_{1-40}$ (**E**) and $A\beta_{1-42}$ (**F** and **G**) in brains from animals at 16 days. The arrows indicate a focal staining of $A\beta_{1-40}$ (**E**) in contrast with more extensive staining of $A\beta_{1-42}$ distributed along with intracellular vesicular structures (blue arrows, **F**), plasma membrane of cell bodies (white arrows, **F**) and also in neurites (blue arrow, **G**). The arrowheads (**G**) point out the co-localization of GFP puncta and $A\beta_{1-42}$ staining. *P* values are two-tailed and obtained by Student's two-tailed *t* test. Scale bars are 5 μm.

foci (Figure 2A). A close examination of $A\beta_{1-40}$ staining reveals that additional $A\beta_{1-40}$-positive signal is localized in regions not coincident with CellMask, but rather present in adjacent areas that may be extracellular spaces (Figure 2A, inserts 1 and 2). $A\beta_{1-42}$ staining in contrast is not found in equivalent areas (Figure 2B, inserts 3 and 4) suggesting that $A\beta_{1-40}$, but not $A\beta_{1-42}$, may be more amenable to secretion into extracellular spaces. To test this possibility directly, we expressed $A\beta_{1-42}$ or $A\beta_{1-40}$ in primary cultured *Drosophila* neurons using a drug-inducible system to conditionally control expression (Supplementary Figures S1C and S1D). Temporal control of expression should minimize confounding factors that might result from specific neuronal toxicity of $A\beta_{1-42}$. Quantification of Aβ in the culture medium or within neurons indicates that $A\beta_{1-40}$ is preferentially recovered from culture medium while $A\beta_{1-42}$ accumulates more prominently within neurons (Figures 2C–2F). These results support the proposal that neurons preferentially retain $A\beta_{1-42}$, likely a

© 2014 The Author(s) This is an Open Access article distributed under the terms of the Creative Commons Attribution Licence (CC-BY) (http://creativecommons.org/licenses/by/3.0/) which permits unrestricted use, distribution and reproduction in any medium, provided the original work is properly cited.

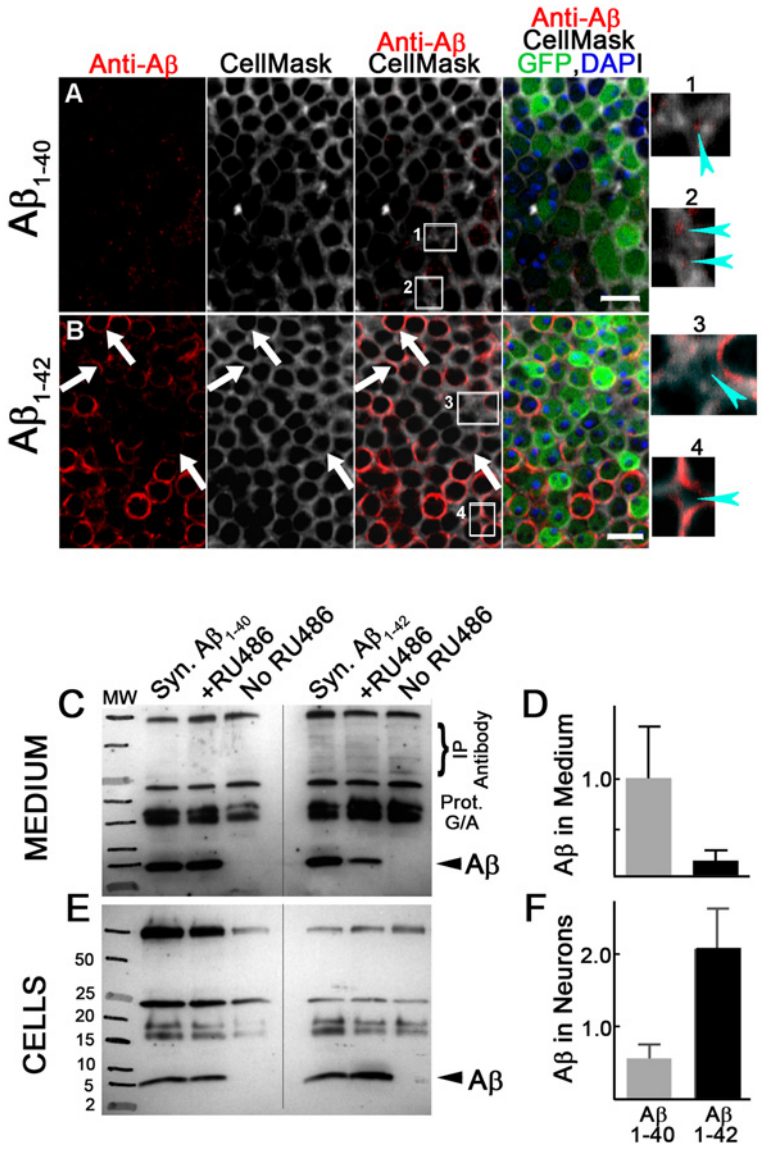

Figure 2 **Aβ species-specific membrane association and secretion**

(**A**, **B**) Fly brains from 1-day-old animals were double-stained with anti-Aβ 4G8 antibody and CellMask, a plasma-membrane-binding fluorescent dye. $Aβ_{1-42}$ staining (**B**) but not $Aβ_{1-40}$ staining (**A**) co-localizes with the CellMask fluorescence. Arrows indicate the close association of $Aβ_{1-42}$ staining with plasma membrane. The small panels on the right (1–4) are magnified views of the indicated regions shown in the CellMask column. $Aβ_{1-40}$ staining (Panels 1–2) but not $Aβ_{1-42}$ staining (Panels 3–4) appears in extracellular spaces where CellMask staining is absent (arrowheads). (**C**–**F**) Representative immunoprecipitation-Western blot images (**C**, **E**) and densitometric analyses ($n = 3$ for **D**, $n = 4$ for **F**) of $Aβ_{1-40}$ and $Aβ_{1-42}$ accumulating in culture medium (**C**, **D**) or within cells (**E**, **F**). Data represent means ± S.D. *P* values are two-tailed and obtained by Student's *t* test. Scale bars are 5 μm.

consequence of its higher membrane affinity, but preferentially release $Aβ_{1-40}$.

Vesicles accumulating punctate GFP and $Aβ_{1-42}$ have endosomal properties

A prominent morphological change induced by $Aβ_{1-42}$, but not $Aβ_{1-40}$, in our *Drosophila* model is a redistribution of the normal homogeneous cytosolic GFP fluorescence into punctate structures (Figures 3A–3C and Supplementary Movie S1 at http://www.asnneuro.org/an/006/an006e139add.htm). Our previous work established that these puncta are derived from an age-dependent autophagic sequestration of cytosolic GFP which is resistant to degradation by lysosomal hydrolases and is thus an indicator of long-lived dysfunctional autophagy–lysosomal vesicles (Ling et al., 2009). In many targeted neurons the contents of these vesicles leaks out into

© 2014 The Author(s) This is an Open Access article distributed under the terms of the Creative Commons Attribution Licence (CC-BY) (http://creativecommons.org/licenses/by/3.0/) which permits unrestricted use, distribution and reproduction in any medium, provided the original work is properly cited.

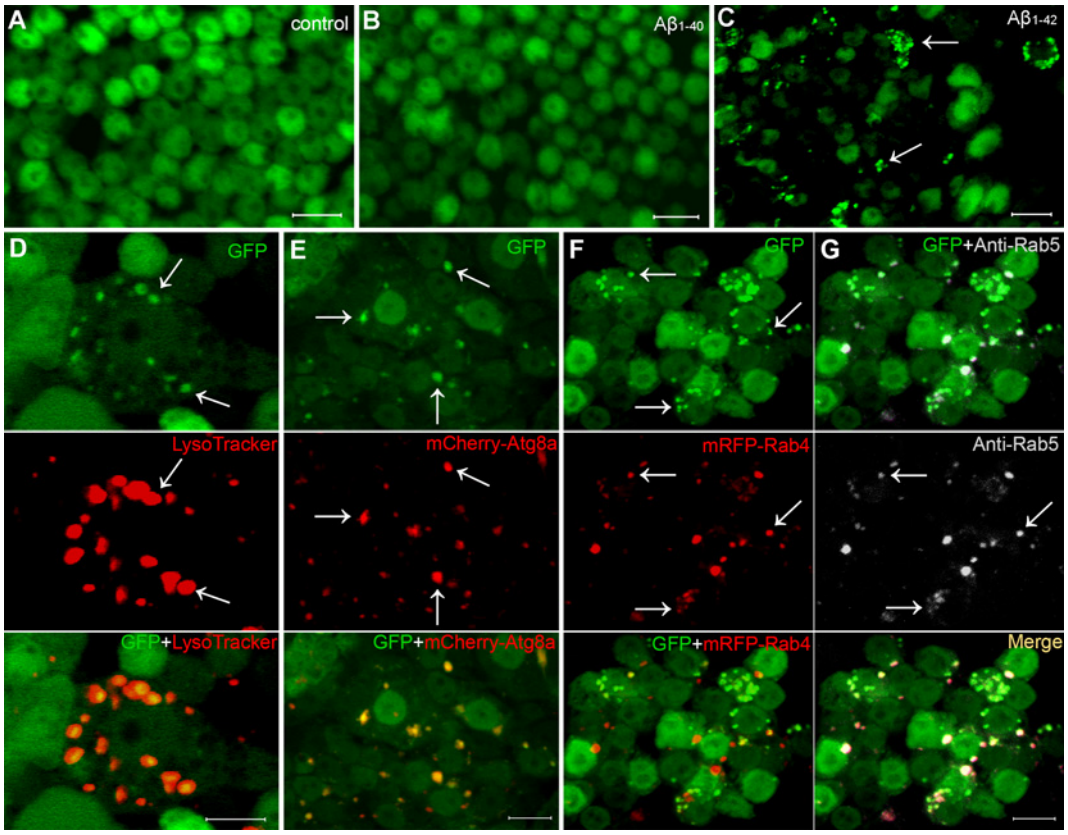

Figure 3 **$A\beta_{1-42}$ expression results in appearance of puncta with characteristic markers of the AEL pathway**
(**A**–**C**) Cytosolic GFP expressed in fly brains exhibits a homogenous distribution in control (**A**, no Aβ expression) or $A\beta_{1-40}$ samples (**B**) but extensive punctate redistribution in $A\beta_{1-42}$ samples (**C**). A 3D animated maximum intensity projection of the GFP fluorescence in the $A\beta_{1-40}$ and $A\beta_{1-42}$ samples shown in (**B**) and (**C**) is included as Supplementary Movie S1 (at http://www.asnneuro.org/an/006/an006e139add.htm). (**D**–**G**) $A\beta_{1-42}$-induced GFP fluorescent puncta (arrows) co-localize with LysoTracker red staining (**D**), transgenic mCherry-Atg8a fluorescence (**E**), transgenic mRFP-Rab4 expression (**F**) and immunostaining of endogenous Rab5 (**G**). Note that the punctate distribution of mRFP-Rab4 co-localizes well with the positive anti-Rab5 immunostaining. Fly age is 16 days, expression controlled by Gad1-Gal4 driver. Scale bars are 5 μm.

cytoplasm where it appears to initiate intraneuronal necrosis and a decrease in the fluorescence intensity of non-vesicular cytosolic GFP, possibly by reactivation of lysosomal hydrolases. This process increases the contrast of non-degraded GFP fluorescence contained within the vesicles relative to surrounding cytosolic GFP fluorescence (Ling et al., 2009; Ling and Salvaterra, 2011b).

Since $A\beta_{1-42}$ is initially associated with plasma membrane and the autophagy and endosomal pathways converge (Eskelinen, 2005), we examined the possible contribution of endosomal involvement in the vesicle compartment recognized by punctuate GFP fluorescence and $A\beta_{1-42}$ staining (Figure 1G). We first confirmed that GFP puncta substantially co-localize with LysoTracker red staining (a lysosomal marker indicating acidic pH, Figure 3D) and transgenic mCherry-labeled autophagy-specific gene 8a protein (mCherry-Atg8a, Figure 3E) identifying the contributions of autophagy and lysosomal vesicle fusion. In addition we observe that most of the GFP puncta also co-localize with transgenic mRFP-labeled Rab4 expression (Figure 3F) as well as anti-Rab5-specific antibody immunostaining (Figure 3G). Rab4 and Rab5 are endosomal markers (Sönnichsen et al., 2000) and these data thus identify the $A\beta_{1-42}$-induced GFP puncta as dysfunctional AEL vesicles. Expression of cytosolic GFP alone or in combination with $A\beta_{1-40}$, in contrast with the $A\beta_{1-42}$ expression, does not result in accumulation of significant numbers of GFP puncta (Figures 3A and 3B and Supplementary Movie S1). Our results thus suggest that $A\beta_{1-42}$, initially associated with plasma membrane, may be transported in part to AEL vesicles through the convergence of endosomal, autophagy and lysosomal structures. The absence of GFP catabolism, evident from its continued fluorescence in the AEL vesicles, along with decreased or absent turnover of the vesicles, appears to be a specific consequence of neuronal $A\beta_{1-42}$ expression, but the specific catabolic inhibitory mechanism remains unknown.

© 2014 The Author(s) This is an Open Access article distributed under the terms of the Creative Commons Attribution Licence (CC-BY) (http://creativecommons.org/licenses/by/3.0/) which permits unrestricted use, distribution and reproduction in any medium, provided the original work is properly cited.

Inefficient vesicle turnover promotes continued fusion of AEL vesicles

Abnormal accumulation of autophagic and endosomal vesicles relevant to AD neuropathology has been postulated to result from a blockage of vesicle fusion with lysosomes, resulting in a failure to acquire catabolic enzymes necessary for cargo degradation (Funk and Kuret, 2012). We co-expressed GFP-Atg8a and mRFP-Rab4 in control, $A\beta_{1-40}$ or $A\beta_{1-42}$ animals to test if the decreased vesicle turnover in $A\beta_{1-42}$-expressing neurons affects the convergence of autophagy and endosomal markers. Compared with age- and brain region-matched control samples with no Aβ expression (Figure 4A) or $A\beta_{1-40}$ samples (Figure 4B), we observe enhanced accumulation of autophagic and endosomal vesicles in $A\beta_{1-42}$ samples (Figures 4C and 4D). Since vesicle turnover is efficient in healthy neurons, this increased accumulation of AEL vesicles in $A\beta_{1-42}$ samples suggests their turnover is slower and that they maintain an extended duration in cytosol. Co-localization of autophagic and endosomal markers is significantly greater in brains from $A\beta_{1-42}$ flies compared with either control or $A\beta_{1-40}$ flies (Figure 4E), suggesting that the decreased vesicle turnover in $A\beta_{1-42}$ samples may actually promote fusion between autophagic and endocytic vesicles. In addition, we frequently observe complex intermediate structures that may be a manifestation of different stages of fusion between the diverse types of AEL vesicles in brain tissue in $A\beta_{1-42}$ samples (Figures 4F and 4I). Some of these appear to be extremely large AEL vesicles (Figures 4J and 4M) that may result from a combination of extended vesicle duration and multiple vesicle fusion among dysfunctional AEL vesicles. In contrast, large AEL vesicles are absent from age-matched control or $A\beta_{1-40}$ samples (Supplementary Figure S2 at http://www.asnneuro.org/an/006/an006e139add.htm).

Decreasing AEL function results in decreased $A\beta_{1-42}$ accumulation

We decreased functional autophagy activity by expressing small interfering RNA transgenes (UAS-RNAi) targeting either autophagy-specific gene 5 ($Atg5^{RNAi}$) or 12 ($Atg12^{RNAi}$) in $A\beta_{1-42}$-expressing neurons. Both RNAi genotypes exhibit a similar reduction in CathD activity (the major lysosomal aspartyl protease; Figure 5A) or the number of LysoTracker-positive structures (Supplementary Figure S3 at http://www.asnneuro.org/an/006/an006e139add.htm) suggesting successful reduction in both the function and catabolic capacity of convergent AEL vesicles. Expression of either RNAi transgene also results in decreased RIPA/SDS-soluble or FA-soluble $A\beta_{1-42}$ accumulation (Figures 5B and 5C). Since the RNAi genotypes do not have significantly different levels of $A\beta_{1-42}$ transcripts relative to control samples, the reduction in $A\beta_{1-42}$ accumulation is likely to be post-transcriptional. The RNAi-mediated decrease in AEL function is limited to $A\beta_{1-42}$-expressing neurons. We additionally used a conventional loss-of-function allele for the autophagy-specific kinase 1 gene ($Atg1^{\Delta 3D}$) that decreases AEL activity in all cell types (Scott et al., 2004). Heterozygous $Atg1^{\Delta 3D}$ animals exhibit decreased CathD activity in fly heads as expected (Figure 5E) and also exhibit a reduction in accumulation of $A\beta_{1-42}$ (Figure 5F). These data suggest the interesting possibility that AEL vesicle formation may be necessary for effective accumulation of $A\beta_{1-42}$ in *Drosophila* neurons. It also seems likely that $A\beta_{1-42}$ may in turn participate in development of the AEL dysfunctional vesicles.

$A\beta_{1-42}$ within AEL vesicles is recognized with aggregate-specific anti-Aβ antibodies

$A\beta_{1-42}$ is an aggregate-prone peptide and its formation into higher-ordered aggregation states is thought to be a key step in development of amyloid plaques in AD. To examine the relationship between dysfunctional AEL vesicles and $A\beta_{1-42}$ amyloid-like aggregation, we performed immunostaining of fly brains using anti-Aβ antibodies that recognize forms of Aβ. Immunostaining with anti-Aβ 4G8 antibody, which does not distinguish between diffuse and aggregated $A\beta_{1-42}$, stains GFP puncta as well as plasma membranes and other types of fibrous-appearing intracellular $A\beta_{1-42}$ structures (Figures 1G and 6A). However, immunostaining with aggregate-specific antibody 7A1a (Zhou et al., 2012) primarily co-localizes with GFP puncta (Figure 6B). A comparison of 4G8 and 7A1a immunostaining thus suggests that highly aggregated forms of $A\beta_{1-42}$ may be limited to the dysfunctional AEL vesicles. This result was further confirmed by immunostaining with a different anti-$A\beta_{1-42}$ antibody (AbCam, ab12267) with reportedly high affinity for plaque-like aggregations of $A\beta_{1-42}$ (http://www.abcam.com/beta-amyloid-1-42-antibody-ab12267.html). The ab12267 immunostaining co-localizes well with many of the AEL vesicles identified by expression of transgenic GFP-Atg8a protein (Figure 6C). Our results thus suggest that aggregated forms of $A\beta_{1-42}$ with potential amyloid-like properties are selectively associated with the dysfunctional AEL vesicles. The non-AEL-localized $A\beta_{1-42}$ is in a non-aggregated state, a result that suggests the vesicles themselves may contribute to amyloid-like aggregation.

AEL vesicles have typical amyloid plaque-like features

This focal aggregation of $A\beta_{1-42}$ specifically within dysfunctional AEL vesicles could be a source of amyloid plaques. To test this, we performed Congo Red histochemical staining on brain sections. Congo Red staining that also exhibits apple-green birefringence is considered to be a 'gold standard' for identification of amyloid plaques in human tissue (Sipe et al., 2010). Brain tissue from $A\beta_{1-42}$ flies, but not age-matched control (Figure 6D) or $A\beta_{1-40}$ flies (Figure 6E), exhibits congophilic staining with typical apple-green birefringence when observed under polarized light microscopy

© 2014 The Author(s) This is an Open Access article distributed under the terms of the Creative Commons Attribution Licence (CC-BY) (http://creativecommons.org/licenses/by/3.0/) which permits unrestricted use, distribution and reproduction in any medium, provided the original work is properly cited.

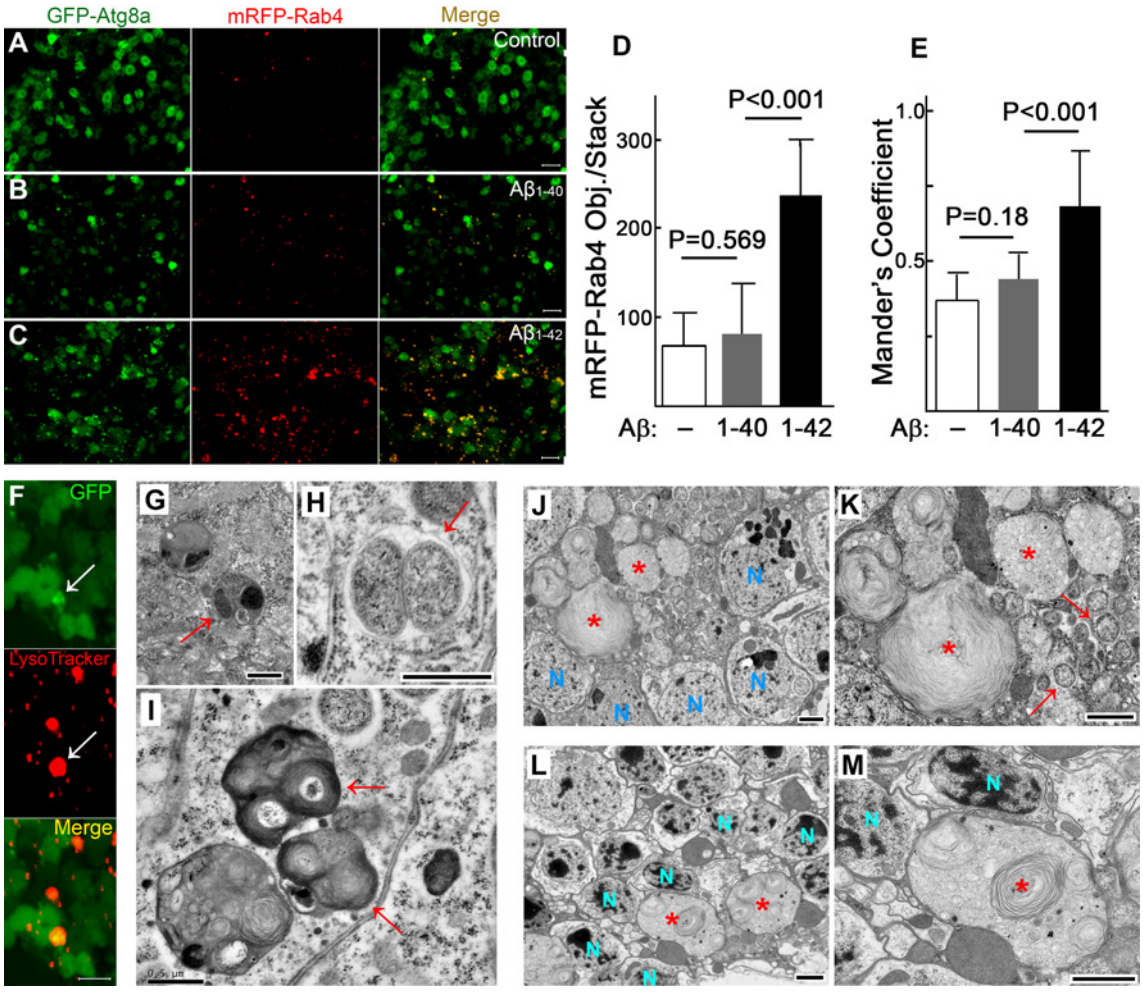

Figure 4 **$A\beta_{1-42}$ expression results in significant fusion of autophagy, lysosomal and endosomal vesicles**

(**A**–**C**) Representative images showing co-localization between mRFP-Rab4 labeled endosomal vesicles and GFP-Atg8a labeled autophagic vesicles in target neurons in brain region- and age-matched control (**A**), $A\beta_{1-40}$ (**B**) and $A\beta_{1-42}$ samples (**C**). Each image represents a maximum intensity projection of a stack of five confocal optical sections with 2 μm of depth. (**D** and **E**) Quantification of the mRFP-Rab4 puncta (**D**) and co-localization assay for mRFP-Rab4 puncta and GFP-Atg8a puncta (**E**) in image stacks. Each data point is from the analysis of nine image stacks collected from three to five individual brains with ten confocal optical sections in each stack (total depth of 4.5 μm). Data are means ± S.D. Two-tailed *P* values obtained by Student's *t* test adjusted for multiple comparisons. (**F**) An AEL vesicle (arrow) likely derived from the apparent fusion of multiple vesicles (distinguishable as individual GFP puncta) with enlarged and unified LysoTracker red staining. Electron micrographs show the fusion of AEL vesicles (**G**–**I**) (arrows) that demonstrates either multiple sources of their contents (**G**), or distinguishable individual small vesicles (**H**), or a clear outline of sub-vesicle structures (**I**). (**J**–**M**) Large AEL vesicles may have developed through a process of continuous or unlimited vesicle fusion. The large AEL vesicles (asterisks) are several times larger than nearby AEL vesicles (**K**, arrows) and occasionally can appear even larger than an adjacent unaffected neuronal cell body (**L** and **M**). (**K**, **M**) is a higher power view of the AEL vesicles in (**J**, **L**). N, nuclei. Fly age = 16 days, expression controlled by Gad1-Gal4 driver. Scale bars are 5 μm (**A**–**C**, **F**), 1 μm (**J**, **L**), or 0.5 μm (**G**–**I**, **K**, **M**).

(Figures 6F and 6G) suggesting an $A\beta_{1-42}$-specific amyloid-type deposition. In addition, the congophilic staining appears to be discrete (Figure 6G) and thus consistent with localization restricted within AEL vesicles. To confirm the association between amyloid formation and AEL vesicles, we applied fluorescent Congo Red staining followed by confocal microscopy as described (Wiesehan et al., 2003). Congo Red fluorescence co-localizes in part with the punctate redistribution of transgenic GFP-Atg8a in $A\beta_{1-42}$ but not $A\beta_{1-40}$-targeted neurons (Figures 6H and 6I). These observations support the possibility that AEL vesicles containing aggregated $A\beta_{1-42}$ deposits could potentially be a source of extracellular amyloid plaques.

AEL vesicles may relocate from intra- to extra-cellular spaces

How could amyloid-containing intracellular AEL vesicles relocate to extracellular spaces? Our previous work showed that compromised AEL vesicles participate in a necrotic-type

© 2014 The Author(s) This is an Open Access article distributed under the terms of the Creative Commons Attribution Licence (CC-BY) (http://creativecommons.org/licenses/by/3.0/) which permits unrestricted use, distribution and reproduction in any medium, provided the original work is properly cited.

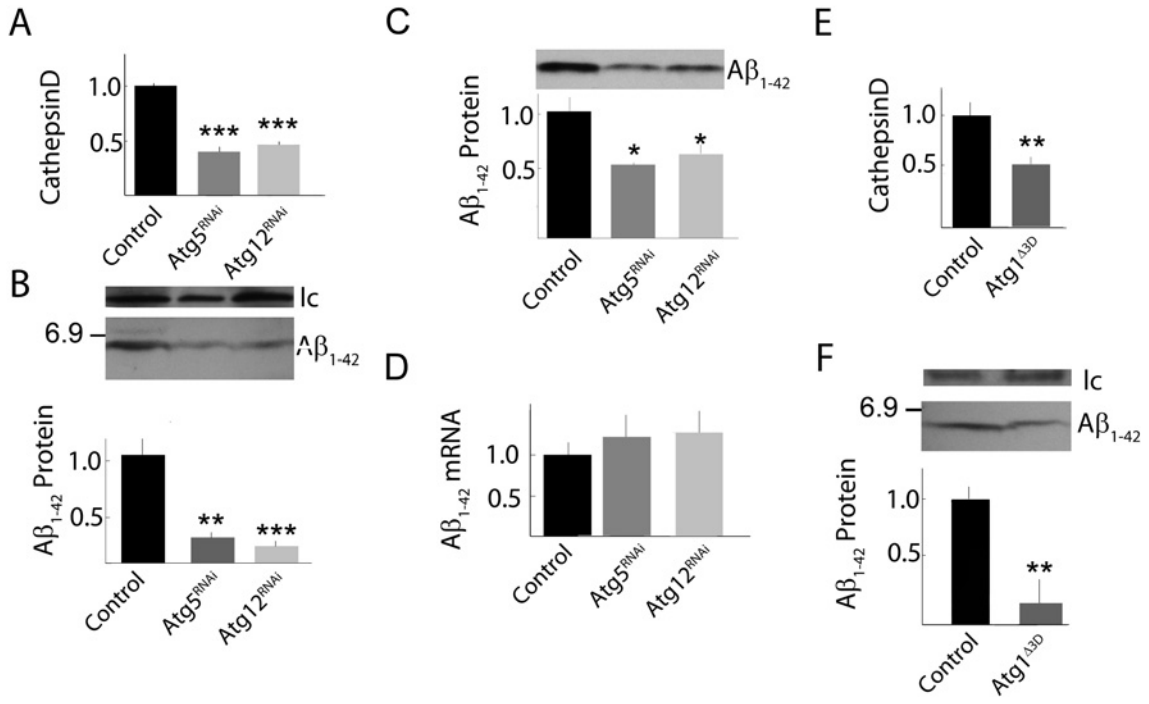

Figure 5 **RNAi or loss-of-function genetic inhibition of autophagy results in decreased $A\beta_{1-42}$ accumulation**

(**A**) Enzymatic activity of CathD is decreased in fly head extracts of samples expressing $Atg5^{RNAi}$ or $Atg12^{RNAi}$ relative to control samples with wild-type autophagy. Interfering RNA against *Atg5* or *Atg12* (RNAi) is targeted to the same neurons expressing $A\beta_{1-42}$. $n = 5$ for each data point. (**B**) Western blot image and densitometric analysis ($n = 5$, bottom) of RIPA/SDS-soluble $A\beta_{1-42}$ accumulation. The loading control (Ic, actin) was used for densitometric normalization. The position of a 6.9 kDa molecular mass marker is indicated. (**C**) Western blot and densitometric analysis ($n = 3$) of RIPA/SDS-insoluble, FA-soluble $A\beta_{1-42}$ accumulation. (**D**) $A\beta_{1-42}$ mRNA levels in fly heads measured by RT–qPCR. Data were normalized to expression levels of *Gapdh*. $n = 3$. (**E**) CathD activity in fly heads with either wild-type autophagy (Control) or heterozygous for an *Atg1* loss-of-function allele ($Atg1^{\Delta 3D}$). $n = 3$. (**F**) Western blot image (top) and densitometric analysis ($n = 3$, bottom) of RIPA/SDS-soluble $A\beta_{1-42}$ accumulation in brains from samples with wild-type autophagy (Control) or heterozygous for *Atg1* loss-of-function ($Atg1^{\Delta 3D}$). All data points are means ± S.E.M. Statistical analysis by ANOVA for (**A**), (**B**) and (**C**) or Student's two-tailed *t* test for (**E**) and (**F**). $^*P < 0.05$,$^{**}P < 0.01$, $^{***}P < 0.001$. Fly age = 5 days. Expression controlled by Cha-Gal4 driver.

neurodegeneration in *Drosophila* (Ling et al., 2009; Ling and Salvaterra, 2011b). Intriguingly, nearly all cytosolic GFP fluorescence in some dying neurons eventually disappears; however, some fluorescent dysfunctional AEL vesicles remain (Figure 7A). This implies that the vesicles containing aggregated amyloid-like forms of $A\beta_{1-42}$ could remain in brain tissue even after the complete necrosis of their host neuron. Consistent with this possibility, we observe clusters of AEL vesicles in extracellular spaces (Figures 7B–7E) that conceivably could have been localized in a now completely degenerated neuron.

The delayed or absent turnover of dysfunctional AEL vesicles, in conjunction with cumulative fusion of additional autophagy and/or endosomal vesicles, also apparently results in the formation of extremely large vesicles which we routinely observe in $A\beta_{1-42}$-expressing samples (Figures 7J–7M), but not in age-matched control or $A\beta_{1-40}$ samples (data not shown). In some cases, these extremely large vesicles appear to be coincident with a process of tortuous infolding of the plasma membrane of their host neuron (Figures 7F and 7G). This infolding process could also conceivably lead to an eventual complete separation of the enlarged vesicles from their resident neuron (Figures 7H and 7I), even in the absence of any neurodegenerative changes in nearby neurons (Figures 7J–7M) and thus result in their appearance in extracellular spaces Similar morphological data is also apparent in very old *Drosophila* even in the absence of $A\beta_{1-42}$ expression and may thus be a consequence of a normal aging process (Ling and Salvaterra, 2011b).

DISCUSSION

Direct expression of $A\beta_{1-42}$ in *Drosophila* neurons is a well-studied model exhibiting many phenotypes with potential relevance to AD (reviewed in Iijima-Ando and Iijima, 2010; Moloney et al., 2009) including decreased lifespan, neurological deficits, amyloid-like deposition in brain, compromise of memory processes and age-dependent neurodegeneration

© 2014 The Author(s) This is an Open Access article distributed under the terms of the Creative Commons Attribution Licence (CC-BY) (http://creativecommons.org/licenses/by/3.0/) which permits unrestricted use, distribution and reproduction in any medium, provided the original work is properly cited.

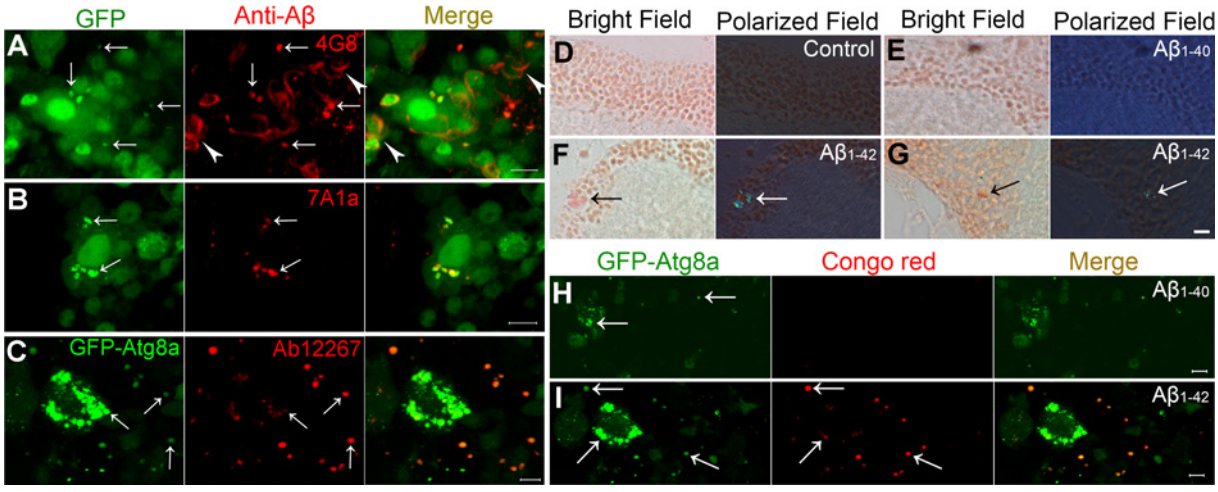

Figure 6 **Selective deposition of amyloid $A\beta_{1-42}$ in AEL vesicles**
(**A–C**) Brains from $A\beta_{1-42}$ flies were immunostained using anti-Aβ antibody 4G8 (**A**), 7A1a (**B**) and Ab12267 (**C**). The arrows indicate co-localization between $A\beta_{1-42}$ staining and GFP puncta (**A**, **B**) or GFP-Atg8a puncta (**C**). Note that the $A\beta_{1-42}$ distribution detected by 4G8 staining is associated with ubiquitous intracellular membranes (**A**, arrowheads). In contrast, there is no additional staining beyond GFP puncta detected by the aggregate-specific 7A1a or the plaque-philic Ab12267 antibody. (**A**) is reused with permission from (Ling et al., 2009). (**D–G**) Brain sections from control (**D**), $A\beta_{1-40}$ (**E**) or $A\beta_{1-42}$ samples (**F**, **G**) are stained with Congo Red and viewed using polarized light. The control and $A\beta_{1-40}$ samples show no congophilic staining. Congophilic staining is detected in $A\beta_{1-42}$ samples (arrows, bright-field) that demonstrate typical apple-green birefringence (arrows, polarized field). Note that the congophilic staining also appears to have a punctate distribution (polarized field, **G**). (**H** and **I**) Brains from $A\beta_{1-40}$ (**H**) and $A\beta_{1-42}$ flies (**I**) were stained by Congo Red and observed using confocal microscopy according to (Wiesehan et al., 2003). The Congo Red fluorescence is observed in $A\beta_{1-42}$ but not $A\beta_{1-40}$ samples and co-localizes with the GFP-Atg8a puncta (arrows) in Aβ-targeted neurons. Fly age is 16 days (**A–C**, **H**, **I**) or 20 days (**D–G**). Scale bars are 5 μm.

(Iijima et al., 2004; Ling et al., 2009). Interestingly, these phenotypes do not usually result from $A\beta_{1-40}$ expression, suggesting underlying $A\beta_{1-42}$-specific neurotoxic mechanisms. One of the most striking cellular differences we observe between $A\beta_{1-42}$ and $A\beta_{1-40}$ is the early age association of $A\beta_{1-42}$ with membrane structures, especially plasma membrane, and this specific association may be a key factor in its specific proteotoxicity in *Drosophila*.

Levels of $A\beta_{1-42}$ versus $A\beta_{1-40}$

The higher $A\beta_{1-42}$ protein immunocytochemical staining we observe in young fly brains compared with $A\beta_{1-40}$ (Figure 1C) is surprising in light of expression of similar transcript levels for these transgenes (Figure 1D). Although this could be a result of technical limitations of whole-brain staining, another possible explanation is that preferential membrane interaction of $A\beta_{1-42}$ may render it resistant to degradation. This possibility has been observed in other systems (Knauer et al., 1992; Burdick et al., 1997; Ling et al., 2009). Our results are also broadly in accordance with AD as well as some mammalian AD models where neurons preferentially produce $A\beta_{1-40}$ from APP proteolysis (Hartmann et al., 1997), but paradoxically accumulate higher levels of intraneuronal $A\beta_{1-42}$ (Gouras et al., 2000, 2005; Laferla et al., 2007). Similar differential accumulation levels have also been previously reported in *Drosophila* photoreceptor neurons (Finelli et al., 2004). The *Drosophila* model thus potentially recapitulates a key feature of AD, the predominant intracellular accumulation of $A\beta_{1-42}$ over $A\beta_{1-40}$. Interestingly, this phenotype is not dependent on amyloidogenic proteolytic processing of APP.

Recycling endocytosis may contribute to accumulation of $A\beta_{1-42}$ in AEL vesicles

Our previous work emphasized a prominent role for dysfunctional autophagy–lysosomal vesicles in $A\beta_{1-42}$ accumulation as well as age-dependent pathogenesis (Ling et al., 2009; Ling and Salvaterra, 2011b). Here we extend these observations by showing that the dysfunctional vesicles also express endosomal markers and thus represent convergent structures of autophagy, endosomal and lysosomal vesicle fusions.

A key question is how endosomal vesicles participate in the specific accumulation of $A\beta_{1-42}$ in the AEL vesicles. We can rule out AEL-dependent processing of APP since the only proteolytic processing necessary for $A\beta_{1-42}$ production in *Drosophila* is removal of the secretory signal peptide during trafficking through the secretory pathway. The complete removal of signal peptide from both $A\beta_{1-40}$ and $A\beta_{1-42}$ in *Drosophila* (Iijima et al., 2004) confirms its successful transit and processing through the secretory pathway. Only $A\beta_{1-42}$, however, associates with plasma membrane, especially at early ages, and specifically accumulates within

© 2014 The Author(s) This is an Open Access article distributed under the terms of the Creative Commons Attribution Licence (CC-BY) (http://creativecommons.org/licenses/by/3.0/) which permits unrestricted use, distribution and reproduction in any medium, provided the original work is properly cited.

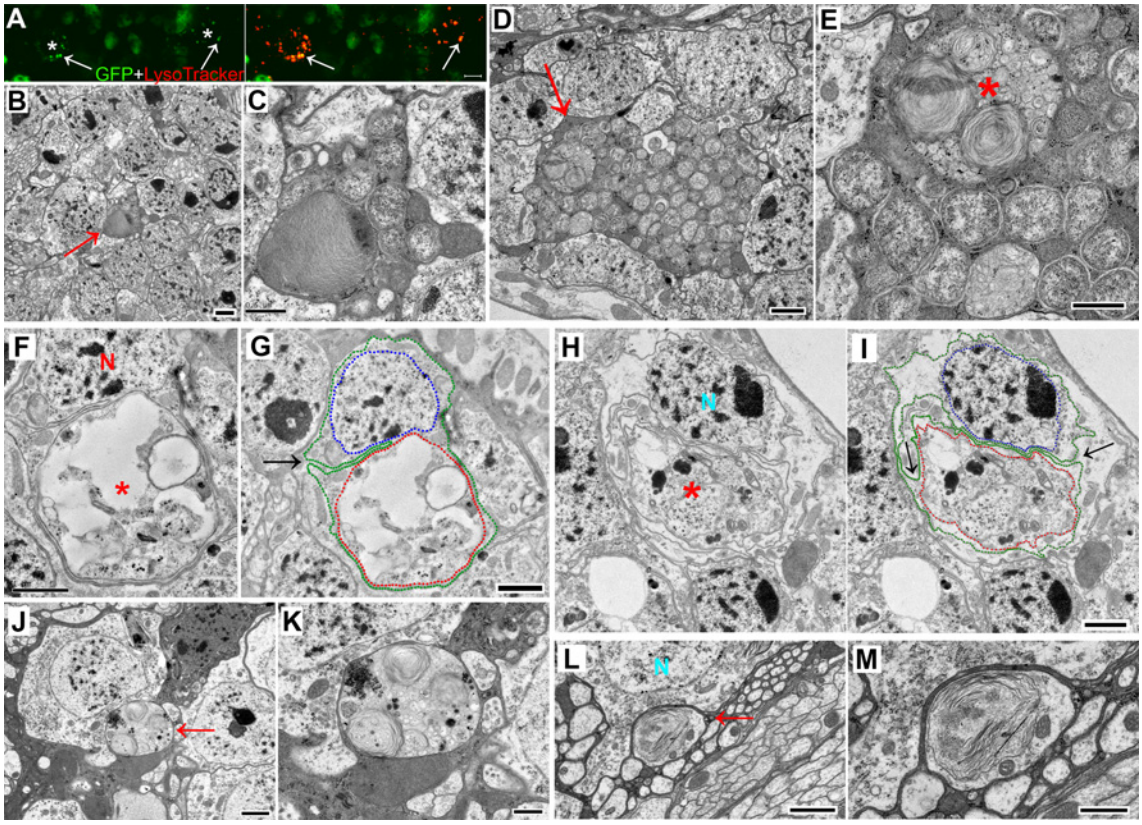

Figure 7 **The AEL vesicles may relocate from intracellular to extracellular spaces**
(**A**) In older (16 day) flies, cytosolic GFP fluorescence in dying neurons (stars) becomes undetectable; however, brightly fluorescent dysfunctional AEL vesicles remain and they co-localize with LysoTracker staining (arrows). (**B**–**E**) Electron micrographs from $A\beta_{1-42}$ flies showing clusters of AEL vesicles present in extracellular spaces (**B** and **D**, arrow; **C** and **E**, higher power view). Note that multiple AEL vesicles appear to be contained within a larger vesicle (**E**, asterisk). A multilamellar structure (**E**, asterisk) indicates a lipidic microenvironment inside the AEL vesicle. (**F** and **G**) A neuron appears to be budding off a large AEL vesicle (**F**, asterisk) through folding of the plasma membrane (**G**, arrow). (**H** and **I**) A large AEL vesicle separated (**H**, star) through plasma membrane infolding (**I**, the arrows). The colored dotted lines (**G**, **I**) trace the plasma membrane (green), the nuclear membrane (blue) and the AEL vesicle membrane (red). (**J**–**M**) Individual large AEL vesicles (**J** and **L**, the arrows) are localized in extracellular spaces. (**K**, **M**) A higher power view of the AEL vesicles. Note that neurons adjacent to these AEL vesicles have no apparent damage. N, nuclei. Fly age = 16 days. Expression controlled by Gad1-Gal4 driver. Scale bars are 5 μm (**A**), 1 μm (**B**, **D**, **J**, **L**) and 0.5 μm (**C**, **E**–**I**, **K**, **M**).

dysfunctional AEL vesicles suggesting that recycling endocytosis of plasma membrane associated $A\beta_{1-42}$ followed by normal endosomal trafficking may at least in part contribute to its accumulation within AEL vesicles. Additional $A\beta_{1-42}$ may also accumulate within AEL vesicles directly as a result of autophagy. This may occur by virtue $A\beta_{1-42}$ association with non-endosomal membrane structures, including mitochondria or non-AEL-related vesicles that are targeted to autophagosomes as part of normal neuronal homoeostatic mechanisms. Non-membrane-associated intracellular $A\beta_{1-42}$ aggregates could also conceivably be targeted directly to the autophagy pathway, but our antibody staining only detects highly aggregated forms of $A\beta_{1-42}$ when they are already incorporated within AEL vesicles, especially in older samples. The reduction in $A\beta_{1-42}$ accumulation we observe following genetic down-regulation of autophagy activity is thus likely to be a consequence of reduced convergence of autophagy and endosomal vesicles. Our genetic results further suggest that AEL vesicles may be necessary for optimal $A\beta_{1-42}$ accumulation in *Drosophila*, a somewhat counterintuitive proposal given the catabolic nature of normal AEL function. We note, however, that the decrease in $A\beta_{1-42}$ accumulation is entirely consistent with our previous genetic observations that autophagy reduction in *Drosophila* lengthens lifespan and reduces the rate of age-dependent neurological deficits while pharmacologically increasing autophagy has an opposite effect in $A\beta_{1-42}$-expressing animals (Ling et al., 2009). Dysfunctional AEL processes may thus not only be necessary for optimal and preferential $A\beta_{1-42}$ accumulation, but also may be necessary for subsequent neurodegenerative mechanism(s) in *Drosophila*.

The relative importance of autophagy, endosomal or lysosomal vesicle trafficking for $A\beta_{1-42}$ accumulation is unknown; however, future genetic studies using endosomal

© 2014 The Author(s) This is an Open Access article distributed under the terms of the Creative Commons Attribution Licence (CC-BY) (http://creativecommons.org/licenses/by/3.0/) which permits unrestricted use, distribution and reproduction in any medium, provided the original work is properly cited.

and autophagy loss-of-function alleles in various combinations could potentially establish this. A recent study has also demonstrated that autophagy inhibition results in decreased Aβ accumulation in mammalian neurons (Nilsson et al., 2013), whereas other studies have found potentially conflicting results (Pickford et al., 2008; Boland et al., 2010). Many of these differences could be a result of various experimental details such as species differences in the type of APP being expressed, the particular types of AEL stimulation or inhibition used, confounding factors related to unspecified amyloidogenic APP processing (i.e. whether $A\beta_{1-42}$ or $A\beta_{1-40}$ predominates) or even the age and stage of neuronal compromise in the cells or neurons being studied. In AD, as well as the majority of mammalian AD models, Aβ must be generated by amyloidogenic proteolytic processing of APP, a process that reportedly occurs at both plasma membrane (Armstrong, 1998; Takahashi et al., 2002b; Marchesi, 2005) as well as intracellular AEL vesicles (Cataldo et al., 2004; Yu et al., 2005). It remains uncertain if either site predominates quantitatively (Haass et al., 2012), but both intracellular and extracellular Aβ are believed to be important for Aβ proteotoxicity as well as intracellular accumulation (Gouras et al., 2005; Mohamed and Posse de Chaves, 2011). Importantly, intracellular Aβ accumulation appears to precede extracellular Aβ deposition as well as plaque formation in some models (Gyure et al., 2001; Knobloch et al., 2007) and $A\beta_{1-42}$ is the primary form of peptide accumulating within mammalian neurons (Laferla et al., 2007), results consistent with our observations in *Drosophila*.

Dysfunctional AEL vesicles may be the source of plaque-like structures

Our previously data (Ling et al., 2009; Ling and Salvaterra, 2011d), as well as data presented here suggest a potential AEL-dependent mechanism for extracellular plaque-like formation in $A\beta_{1-42}$-expressing *Drosophila*. First, APP amyloidogenic proteolysis is not necessary. Both recycling endocytosis as well as autophagy could provide the necessary routes for $A\beta_{1-42}$ accumulation within AEL vesicle compartments and the relative selectivity of $A\beta_{1-42}$ over $A\beta_{1-40}$ could result from its greater membrane association. In young animals, the $A\beta_{1-42}$-containing AEL vesicles are capable of cargo digestion and would thus turnover at an appreciable rate. Aged animals, however, have a decreased efficiency for cargo degradation as a consequence of normal aging processes (Cuervo et al., 2005). In $A\beta_{1-42}$-expressing *Drosophila* neurons the dysfunctional AEL vesicles persist for long durations, continue to fuse with additional endocytic, autophagic and lysosomal vesicles and can become extremely large. Since $A\beta_{1-42}$ is also present in non-AEL locations in a non-amyloid form in *Drosophila* neurons, *in vivo* accumulation of $A\beta_{1-42}$ alone does not appear to be sufficient for amyloid formation. Amyloid formation may rather be dependent on the acidic and lipidic microenvironment of AEL vesicles, conditions shown to be favorable for formation of toxic aggregated forms of Aβ in mammalian neurons (Su and Chang, 2001). We have previously shown that some AEL vesicles leak their contents into cytoplasm (Ling et al., 2009). This process might conceivably create a non-AEL acidic and lipidic microenvironment in cytoplasm that could also convert non-amyloid $A\beta_{1-42}$ into an amyloid-like form that is subsequently reincorporated into AEL vesicles. Finally, dysfunctional AEL vesicles containing amyloid-like $A\beta_{1-42}$ would be relocated to extracellular spaces by two distinct mechanisms: neurodegeneration itself or separation of large dysfunctional AEL vesicles through a process of plasma membrane infolding.

The origin of extracellular senile plaques in AD is still a matter of debate. A prevalent view holds that they are formed by an autonomous condensation of extracellular Aβ peptides released from plasma membrane proteolysis of APP (Armstrong, 1998; Fiala, 2007). Alternative views emphasize an intracellular origin, including generation of Aβ directly by AEL vesicles (Glabe, 2001). Our proposed AEL-relocalization model in *Drosophila* may also have relevance for AD and mammalian AD models (Takahashi et al., 2002a; D'Andrea et al., 2003). The congophilic staining in *Drosophila* is discrete and consistent with amyloid restriction to a vesicular structure. Similar microdeposits have been observed in aged transgenic mouse brains expressing mutant APP (Takahashi et al., 2004; Stokin et al., 2005). The long duration and continuing fusion of membrane vesicles involved in AEL formation could easily result in production of not only large-sized amyloid plaques, but also a diversity of plaques sizes with spherical shapes, a common feature of AD and other AD models including our *Drosophila* AD model (Fiala, 2007; Ling et al., 2009; Ling and Salvaterra, 2011b). This proposed plaque model is also consistent with lysosomal materials, damaged organelles and other intracellular contents associated with AD plaques (Suzuki and Terry, 1967; Cataldo and Nixon, 1990; Fiala, 2007). It could obviate the difficulties in reconciling the different proportions of Aβ species found in diffuse, primitive and mature dense-core plaques (Fiala, 2007) believed to represent different stages of extracellular plaque maturation (Armstrong, 1998) with observations that senile plaques themselves contain primarily $A\beta_{1-42}$. The model could even explain why Aβ is constitutively produced in human brain and peripheral tissues from fetal stages to old age (Wegiel et al., 2007), but amyloid deposition, as well as plaque formation, are generally absent in young people. It is also consistent with the absence of plaques when non-secretory $A\beta_{1-42}$ is expressed directly in mammalian neuronal cytosol (Jucker et al., 1992; LaFerla et al., 1995) as well as studies showing that both internalization of extracellular Aβ as well as plasma membrane binding are necessary for toxicity in various types of cultured mammalian cells and neurons, and that endocytosis appears to play an essential role in this toxicity (Simakova and Arispe, 2007; Friedrich et al., 2010). Finally, our proposal agrees with the recent observations that autophagy may be necessary for plaque formation in a transgenic mouse model of AD that is dependent on amyloidogenic APP processing (Nilsson et al., 2013).

© 2014 The Author(s) This is an Open Access article distributed under the terms of the Creative Commons Attribution Licence (CC-BY) (http://creativecommons.org/licenses/by/3.0/) which permits unrestricted use, distribution and reproduction in any medium, provided the original work is properly cited.

AUTHOR CONTRIBUTION

Daijun Ling and Paul Salvaterra contributed to the experimental design and preparation of the manuscript. Daijun Ling, Paul Salvaterra and Martha Magallanes participated in data collection and analysis.

ACKNOWLEDGEMENTS

We thank Dr Thomas P. Neufeld (University of Minnesota), Dr Haig Keshishian (Yale University), and Bloomington Stock Center for providing *Drosophila* lines, Maria De La O (City of Hope) for preparation of brain sections and Congo Red staining, and Elvia Gutierrez (City of Hope) for general technical support. The authors declare no financial conflict of interest.

FUNDING

This work was supported by the Sidell-Kagan Foundation and the American Health Assistance Foundation (to P.M.S.), as well as a fellowship from the American Federation for Aging Research (to D.L).

REFERENCES

Armstrong RA (1998) Beta-amyloid plaques: stages in life history or independent origin? Dement Geriatr Cogn Disord 9:227–238.

Boland B, Smith D, Mooney D, Jung SS, Walsh DM, Platt FM (2010) Macroautophagy is not directly involved in the metabolism of amyloid precursor protein. J Biol Chem 285:37415–37426.

Burdick D, Kosmoski J, Knauer MF, Glabe CG (1997) Preferential adsorption, internalization and resistance to degradation of the major isoform of the Alzheimer's amyloid peptide, Aβ 1–42, in differentiated PC12 cells. Brain Res 746:275–284.

Cataldo AM, Nixon RA (1990) Enzymatically active lysosomal proteases are associated with amyloid deposits in Alzheimer brain. Proc Natl Acad Sci USA 87:3861–3865.

Cataldo AM, Petanceska S, Terio NB, Peterhoff CM, Durham R, Mercken M, Mehta PD, Buxbaum J, Haroutunian V, Nixon RA (2004) Abeta localization in abnormal endosomes: association with earliest Abeta elevations in AD and Down syndrome. Neurobiol Aging 25:1263–1272.

Chang Y-Y, Neufeld TP (2009) An Atg1/Atg13 complex with multiple roles in TOR-mediated autophagy regulation. Mol Biol Cell 20:2004–2014.

Cuervo AM, Bergamini E, Brunk UT, Droge W, Ffrench M, Terman A (2005) Autophagy and aging: the importance of maintaining "clean" cells. Autophagy 1:131–140.

D'Andrea MR, Reiser PA, Polkovitch DA, Gumula NA, Branchide B, Hertzog BM, Schmidheiser D, Belkowski S, Gastard MC, Andrade-Gordon P (2003) The use of formic acid to embellish amyloid plaque detection in Alzheimer's disease tissues misguides key observations. Neurosci Lett 342:114–118.

Eskelinen EL (2005) Maturation of autophagic vacuoles in mammalian cells. Autophagy 1:1–10.

Fiala JC (2007) Mechanisms of amyloid plaque pathogenesis. Acta Neuropathol 114:551–571.

Finelli A, Kelkar A, Song HJ, Yang H, Konsolaki M (2004) A model for studying Alzheimer's Abeta42-induced toxicity in *Drosophila melanogaster*. Mol Cell Neurosci 26:365–375.

Friedrich RP, Tepper K, Ronicke R, Soom M, Westermann M, Reymann K, Kaether C, Fandrich M (2010) Mechanism of amyloid plaque formation suggests an intracellular basis of Abeta pathogenicity. Proc Natl Acad Sci USA 107:1942–1947.

Funk KE, Kuret J (2012) Lysosomal fusion dysfunction as a unifying hypothesis for Alzheimer's disease pathology. Int J Alzheimers Dis 2012:752894.

Funk KE, Mrak RE, Kuret J (2011) Granulovacuolar degeneration (GVD) bodies of Alzheimer's disease (AD) resemble late-stage autophagic organelles. Neuropathol Appl Neurobiol 37:295–306.

Glabe C (2001) Intracellular mechanisms of amyloid accumulation and pathogenesis in Alzheimer's disease. J Mol Neurosci 17:137–145.

Gouras GK, Almeida CG, Takahashi RH (2005) Intraneuronal Abeta accumulation and origin of plaques in Alzheimer's disease. Neurobiol Aging 26:1235–1244.

Gouras GK, Tsai J, Naslund J, Vincent B, Edgar M, Checler F, Greenfield JP, Haroutunian V, Buxbaum JD, Xu H, Greengard P, Relkin NR (2000) Short Communication. Am J Pathol 156:15–20.

Gyure KA, Durham R, Stewart WF, Smialek JE, Troncoso JC (2001) Intraneuronal abeta-amyloid precedes development of amyloid plaques in Down syndrome. Arch Pathol Lab Med 125:489–492.

Haass C, Kaether C, Thinakaran G, Sisodia S (2012) Trafficking and proteolytic processing of APP. Cold Spring Harb Perspect Med 2:a006270.

Hartmann T, Bieger SC, Bruhl B, Tienari PJ, Ida N, Allsop D, Roberts GW, Masters CL, Dotti CG, Unsicker K, Beyreuther K (1997) Distinct sites of intracellular production for Alzheimer's disease A beta40/42 amyloid peptides. Nat Med 3:1016–1020.

Hu X, Pickering E, Liu YC, Hall S, Fournier H, Katz E, Dechairo B, John S, Van Eerdewegh P, Soares H (2011a) Meta-analysis for genome-wide association study identifies multiple variants at the BIN1 locus associated with late-onset Alzheimer's disease. PLoS One 6:e16616.

Hu X, Pickering EH, Hall SK, Naik S, Liu YC, Soares H, Katz E, Paciga SA, Liu W, Aisen PS, Bales KR, Samad TA, John SL (2011b) Genome-wide association study identifies multiple novel loci associated with disease progression in subjects with mild cognitive impairment. Transl Psychiatry 1:e54.

Iijima K, Liu H-PP, Chiang A-SS, Hearn SA, Konsolaki M, Zhong Y (2004) Dissecting the pathological effects of human Abeta40 and Abeta42 in *Drosophila*: a potential model for Alzheimer's disease. Proc Natl Acad Sci USA 101:6623–6628.

Iijima-Ando K, Iijima K (2010) Transgenic *Drosophila* models of Alzheimer's disease and tauopathies. Brain Struct Funct 214:245–262.

Jucker M, Walker LC, Martin LJ, Kitt CA, Kleinman HK, Ingram DK, Price DL (1992) Age-associated inclusions in normal and transgenic mouse brain. Science 255:1443–1445.

Knauer MF, Soreghan B, Burdick D, Kosmoski J, Glabe CG (1992) Intracellular accumulation and resistance to degradation of the Alzheimer amyloid A4/beta protein. Proc Natl Acad Sci USA 89:7437–7441.

Knobloch M, Konietzko U, Krebs DC, Nitsch RM (2007) Intracellular Abeta and cognitive deficits precede beta-amyloid deposition in transgenic arcAbeta mice. Neurobiol Aging 28:1297–1306.

Laferla FM, Green KN, Oddo S (2007) Intracellular amyloid-beta in Alzheimer's disease. Nat Rev Neurosci 8:499–509.

LaFerla FM, Tinkle BT, Bieberich CJ, Haudenschild CC, Jay G (1995) The Alzheimer's A beta peptide induces neurodegeneration and apoptotic cell death in transgenic mice. Nat Genet 9:21–30.

Li Q, Lau A, Morris TJ, Guo L, Fordyce CB, Stanley EF (2004) A syntaxin 1, Galpha(o), and N-type calcium channel complex at a presynaptic nerve terminal: analysis by quantitative immunocolocalization. J Neurosci 24:4070–4081.

Ling D (2012) SASqPCR: robust and rapid analysis of RT-qPCR data in SAS. PLoS One 7:e29788.

Ling D, Pike CJ, Salvaterra PM (2012) Deconvolution of the confounding variations for reverse transcription quantitative real-time polymerase chain reaction by separate analysis of biological replicate data. Anal Biochem 427:21–25.

Ling D, Salvaterra PM (2011a) Autophagy-derived Alzheimer's pathogenesis. In: Alzheimer's Disease Pathogenesis-Core Concepts, Shifting Paradigms and Therapeutic Targets (De La Monte S, ed.), pp. 539–560, InTech.

Ling D, Salvaterra PM (2011b) Brain aging and Aβ1–42 neurotoxicity converge via deterioration in autophagy-lysosomal system: a conditional *Drosophila* model linking Alzheimer's neurodegeneration with aging. Acta Neuropathol 121:183–191.

© 2014 The Author(s) This is an Open Access article distributed under the terms of the Creative Commons Attribution Licence (CC-BY) (http://creativecommons.org/licenses/by/3.0/) which permits unrestricted use, distribution and reproduction in any medium, provided the original work is properly cited.

Ling D, Salvaterra PM (2011c) Robust RT-qPCR data normalization: validation and selection of internal reference genes during post-experimental data analysis. PLoS One 6:e17762.

Ling D, Salvaterra PM (2011d) Autophagy-derived Alzheimer's Pathogenesis. In: Alzheimer's Disease Pathogenesis-Core Concepts, Shifting Paradigms and Therapeutic Targets (Monte SD La, ed). InTech.

Ling D, Song H-J, Garza D, Neufeld TP, Salvaterra PM (2009) Abeta42-induced neurodegeneration via an age-dependent autophagic-lysosomal injury in *Drosophila*. PLoS One 4:e4201.

Liou W, Geuze HJ, Geelen MJ, Slot JW (1997) The autophagic and endocytic pathways converge at the nascent autophagic vacuoles. J Cell Biol 136:61–70.

Manjithaya R, Subramani S (2011) Autophagy: a broad role in unconventional protein secretion? Trends Cell Biol 21:67–73.

Marchesi VT (2005) An alternative interpretation of the amyloid Abeta hypothesis with regard to the pathogenesis of Alzheimer's disease. Proc Natl Acad Sci USA 102:9093–9098.

Maxfield FR, McGraw TE (2004) Endocytic recycling. Nat Rev Mol Cell Biol 5:121–132.

Mohamed A, Posse de Chaves E (2011) Aβ internalization by neurons and glia. Int J Alzheimers Dis 2011:127984.

Moloney A, Sattelle DB, Lomas DA, Crowther DC (2009) Alzheimer's disease: insights from *Drosophila melanogaster* models. Trends Biochem Sci 35:228–235.

Naj AC, Jun G, Beecham GW, Wang LS, Vardarajan BN, Buros J, Gallins PJ, Buxbaum JD, Jarvik GP, Crane PK et al. (2011) Common variants at MS4A4/MS4A6E, CD2AP, CD33 and EPHA1 are associated with late-onset Alzheimer's disease. Nat Genet 43:436–441.

Nilsson P, Loganathan K, Sekiguchi M, Matsuba Y, Hui K, Tsubuki S, Tanaka M, Iwata N, Saito T, Saido TC (2013) Aβ secretion and plaque formation depend on autophagy. Cell Rep 7:1–9.

Nixon RA (2005) Endosome function and dysfunction in Alzheimer's disease and other neurodegenerative diseases. Neurobiol Aging 26:373–382.

Nixon RA, Wegiel J, Kumar A, Yu WH, Peterhoff C, Cataldo A, Cuervo AM (2005) Extensive involvement of autophagy in Alzheimer disease: an immuno-electron microscopy study. J Neuropathol Exp Neurol 64:113–122.

Okamoto K, Hirai S, Iizuka T, Yanagisawa T, Watanabe M (1991) Reexamination of granulovacuolar degeneration. Acta Neuropathol 82:340–345.

Perl DPD (2010) Neuropathology of Alzheimer's disease. Mt Sinai J Med 77:32–42.

Pickford F, Masliah E, Britschgi M, Lucin K, Narasimhan R, Jaeger PA, Small S, Spencer B, Rockenstein E, Levine B, Wyss-Coray T (2008) The autophagy-related protein beclin 1 shows reduced expression in early Alzheimer disease and regulates amyloid beta accumulation in mice. J Clin Invest 118:2190–2199.

Saftig P, Klumperman J (2009) Lysosome biogenesis and lysosomal membrane proteins: trafficking meets function. Nat Rev Mol Cell Biol 10: 623–635.

Salvaterra P, Hayashi I, Ikeda K (1998) Primary culture of *Drosophila* embryo cells. In: Celis JE (Ed.), Cell Biology: A Laboratory Handbook, Vol. 1 Academic Press, New York, pp 393–397.

Scott RC, Schuldiner O, Neufeld TP (2004) Role and regulation of starvation-induced autophagy in the *Drosophila* fat body. Dev Cell 7:167–178.

Simakova O, Arispe NJ (2007) The cell-selective neurotoxicity of the Alzheimer's Abeta peptide is determined by surface phosphatidylserine and cytosolic ATP levels. Membrane binding is required for Abeta toxicity. J Neurosci 27:13719–13729.

Sipe JD, Benson MD, Buxbaum JN, Ikeda S-I, Merlini G, Saraiva MJM, Westermark P (2010) Amyloid fibril protein nomenclature: 2010 recommendations from the nomenclature committee of the International Society of Amyloidosis. Amyloid 17:101–104.

Sönnichsen B, De Renzis S, Nielsen E, Rietdorf J, Zerial M (2000) Distinct membrane domains on endosomes in the recycling pathway visualized by multicolor imaging of Rab4, Rab5, and Rab11. J Cell Biol 149:901–914.

Stokin GB, Lillo C, Falzone TL, Brusch RG, Rockenstein E, Mount SL, Raman R, Davies P, Masliah E, Williams DS, Goldstein LSB (2005) Axonopathy and transport deficits early in the pathogenesis of Alzheimer's disease. Science 307:1282–1288.

Su Y, Chang PT (2001) Acidic pH promotes the formation of toxic fibrils from beta-amyloid peptide. Brain Res 893:287–291.

Suzuki K, Terry RD (1967) Fine structural localization of acid phosphatase in senile plaques in Alzheimer's presenile dementia. Acta Neuropathol 8:276–284.

Takahashi RH, Almeida CG, Kearney PF, Yu F, Lin MT, Milner TA, Gouras GK (2004) Oligomerization of Alzheimer's beta-amyloid within processes and synapses of cultured neurons and brain. J Neurosci 24:3592–3599.

Takahashi RH, Milner TA, Li F, Nam EE, Edgar MA, Yamaguchi H, Beal MF, Xu H, Greengard P, Gouras GK (2002a) Intraneuronal Alzheimer abeta42 accumulates in multivesicular bodies and is associated with synaptic pathology. Am J Pathol 161:1869–1879.

Takahashi RH, Nam EE, Edgar M, Gouras GK (2002b) Alzheimer beta-amyloid peptides: normal and abnormal localization. Histol Histopathol 17:239–246.

Wegiel JJ, Kuchna I, Nowicki K, Frackowiak J, Mazur-Kolecka B, Imaki H, Wegiel J, Mehta PD, Silverman WP, Reisberg B, Deleon M, Wisniewski T, Pirttilla T, Frey H, Lehtimäki T, Kivimäki T, Visser FE, Kamphorst W, Potempska A, Bolton D, Currie JR, Miller DL (2007) Intraneuronal Abeta immunoreactivity is not a predictor of brain amyloidosis-beta or neurofibrillary degeneration. Acta Neuropathol 113:389–402.

Wiesehan K, Buder K, Linke RP, Patt S, Stoldt M, Unger E, Schmitt B, Bucci E, Willbold D (2003) Selection of D-amino-acid peptides that bind to Alzheimer's disease amyloid peptide abeta1–42 by mirror image phage display. Chembiochem 4:748–753.

Wilcock DM, Gordon MN, Morgan D (2006) Quantification of cerebral amyloid angiopathy and parenchymal amyloid plaques with Congo red histochemical stain. Nat Protoc 1:1591–1595.

Yasuda Y, Kageyama T, Akamine A, Shibata M, Kominami E, Uchiyama Y, Yamamoto K (1999) Characterization of new fluorogenic substrates for the rapid and sensitive assay of cathepsin E and cathepsin D. J Biochem 125:1137–1143.

Yu WH, Cuervo AM, Kumar A, Peterhoff CM, Schmidt SD, Lee J-H, Mohan PS, Mercken M, Farmery MR, Tjernberg LO, Jiang Y, Duff K, Uchiyama Y, Näslund J, Mathews PM, Cataldo AM, Nixon RA, Naslund J (2005) Macroautophagy: a novel Beta-amyloid peptide-generating pathway activated in Alzheimer's disease. J Cell Biol 171:87–98.

Zhou L, Chan KH, Chu LW, Kwan JSC, Song YQ, Chen LH, Ho PWL, Cheng OY, Ho JWM, Lam KSL (2012) Plasma amyloid-β oligomers level is a biomarker for Alzheimer's disease diagnosis. Biochem Biophys Res Commun 423:697–702.

Received 14 October 2013/8 February 2014; accepted 11 February 2014

Published as Immediate Publication 12 February 2014, doi 10.1042/AN20130044

© 2014 The Author(s) This is an Open Access article distributed under the terms of the Creative Commons Attribution Licence (CC-BY) (http://creativecommons.org/licenses/by/3.0/) which permits unrestricted use, distribution and reproduction in any medium, provided the original work is properly cited.

ASN NEURO RESEARCH ARTICLE

Supplementary data multimedia

ASN NEURO 6(2):art:e00139.doi:10.1042/AN20130044

OPEN ACCESS

Accumulation of amyloid-like $A\beta_{1-42}$ in AEL (autophagy–endosomal–lysosomal) vesicles: potential implications for plaque biogenesis

Daijun Ling*[1], Martha Magallanes* and Paul M. Salvaterra*†[1]

*Department of Neuroscience, Beckman Research Institute of City of Hope, Duarte, CA 91010, U.S.A.

†Irell and Manella Graduate School of Biological Sciences, City of Hope, Duarte, CA 91010, U.S.A.

SUPPLEMENTARY DATA

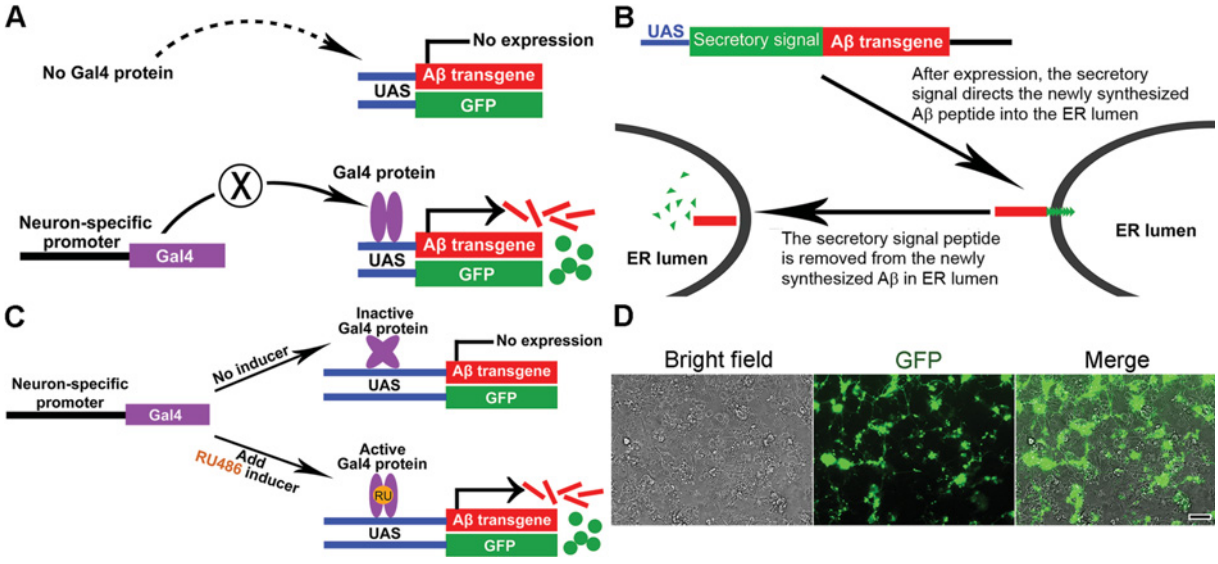

Figure S1 ***In vivo* and *in vitro* expression of secretory human $A\beta_{1-40}$ or $A\beta_{1-42}$ in *Drosophila* neurons**

(**A**) Schematic illustration of neuron-specific expression of Aβ and GFP in *Drosophila* using the bipartite Gal4-UAS method. We used two different neuron-specific promoters fused to Gal4 in this study: a 3.1 kb Gad1-Gal4 transgene expressed only in GABAergic neurons or a 7.4 kb Cha-Gal4 transgene expressed only in cholinergic neurons. Either promoter drives expression in a large number of CNS neurons and both have been previously described (Ling et al., 2009). The driver stocks are genetically recombined with UAS-responder transgenes (i.e. UAS-Aβ containing a secretory signal sequence, UAS-GFP or UAS-fluorescently labeled fusion proteins). (**B**) Schematic illustration of the normal cellular processing of the Aβ secretory signal peptide. The peptide is completely removed when these constructs are expressed in *Drosophila* neurons (Iijima et al., 2004). Both $A\beta_{1-42}$ and $A\beta_{1-40}$ can then be freely secreted from the ER lumen. See a more detailed description in the Materials and Methods section of the main text. (**C**) Schematic illustration of mifepristone (RU486) inducible Gal4-UAS GeneSwitch method used to control temporal and neuron-specific expression of Aβ transgenes as previous described (Nicholson et al., 2008; Ling and Salvaterra, 2011b) and used in the cultured neuron experiments. (**D**) Representative images of primary cultured neurons. Expression of cytosolic GFP indicates an effective RU486 induction of transgenic neuronal Gal4 expression. Scale bar is 50 μm.

[1] Correspondence may be addressed to either of these authors (email psalv@coh.org or lingdaijun@gmail.com).

© **2014 The Author(s)** This is an Open Access article distributed under the terms of the Creative Commons Attribution Licence (CC-BY) (http://creativecommons.org/licenses/by/3.0/) which permits unrestricted use, distribution and reproduction in any medium, provided the original work is properly cited.

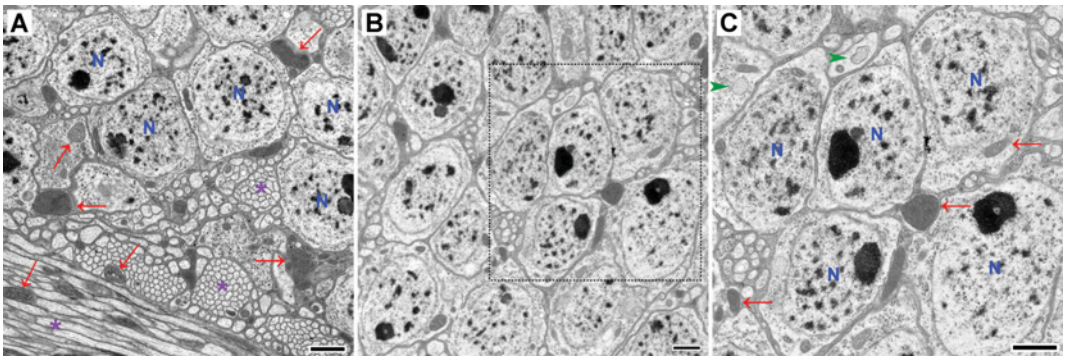

Figure S2 **Representative electron micrographs of neurons from control samples (no Aβ expression) or $A\beta_{1-40}$-expressing samples**
(**A**) Control. (**B** and **C**) $A\beta_{1-40}$. (**C**) A higher magnification view of the square area indicated in (**B**). Note that the most prominent organelles in the cytoplasm of all three images appear to be mitochondria (arrows). No AEL vesicles are visible in control samples (**A**) and only a few small structures with the characteristic appearance of AEL vesicles are observed in intracellular spaces in (**C**, arrowheads). N, nucleus; asterisk, an axonal bundle. Fly age is 16 days. Scale bars are 1 μm.

© 2014 The Author(s) This is an Open Access article distributed under the terms of the Creative Commons Attribution Licence (CC-BY) (http://creativecommons.org/licenses/by/3.0/) which permits unrestricted use, distribution and reproduction in any medium, provided the original work is properly cited.

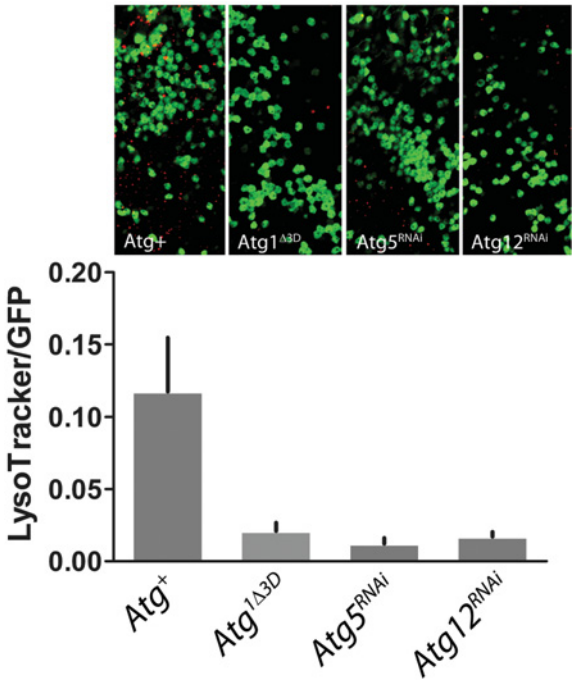

Figure S3 Functional inhibition of autophagy decreases LysoTracker red staining

Freshly dissected whole fly brains were incubated in PBS containing 0.5 μM LysoTracker red (Molecular Probes) for 5 min, washed twice with PBS and immediately observed using confocal microscopy (Zeiss LSM 510). Z-stacks of images were obtained using the green channel for GFP and the red channel for LysoTracker with a 63× (NA = 1.2) water-immersion objective. Image quantification for LysoTracker-positive objects was performed using ImageProPlus (Media Cybernetics). The experimenter was blinded to sample identities relevant to experimental conditions and independent observations were made on four individual brains for each experimental condition. The fluorescence area of LysoTracker-positive staining was normalized to the GFP fluorescence. Bars represent the mean normalized LysoTracker signal derived from analysis of at least ten optical sections from each brain. Error bars are S.E.M. ($n = 4$). The *Atg1*$^{\Delta 3D}$ heterozygotes as well as either RNAi genotype have decreased autophagy function and show less LysoTracker staining compared with the $A\beta_{1-42}$-expressing control sample with normal autophagy function (*Atg*$^{+}$). $P < 0.01$, ANOVA, Bonferoni correction for multiple comparisons. Fly age = 10 days, expression controlled by Gad1-Gal4 driver. LysoTracker staining apparently not associated with obvious GFP fluorescence is due to a combination of staining in non-targeted cells as well as weak or absent GFP fluorescence in cytoplasm of degenerating targeted neurons.

REFERENCES

Iijima K, Liu H-PP, Chiang A-SS, Hearn SA, Konsolaki M, Zhong Y (2004) Dissecting the pathological effects of human Abeta40 and Abeta42 in *Drosophila*: a potential model for Alzheimer's disease. Proc Natl Acad Sci USA 101:6623–6628.

Ling D, Song H-J, Garza D, Neufeld TP, Salvaterra PM (2009) Abeta42-induced neurodegeneration via an age-dependent autophagic-lysosomal injury in *Drosophila*. PLoS One 4:e4201.

Ling D, Salvaterra PM (2011b) Brain aging and Aβ1–42 neurotoxicity converge via deterioration in autophagy-lysosomal system: a conditional *Drosophila* model linking Alzheimer's neurodegeneration with aging. Acta Neuropathol 121:183–191.

Nicholson L, Singh GK, Osterwalder T, Roman GW, Davis RL, Keshishian H (2008) Spatial and temporal control of gene expression in *Drosophila* using the inducible GeneSwitch GAL4 system. I. Screen for larval nervous system drivers. Genetics 178:215–234.

© 2014 The Author(s) This is an Open Access article distributed under the terms of the Creative Commons Attribution Licence (CC-BY) (http://creativecommons.org/licenses/by/3.0/) which permits unrestricted use, distribution and reproduction in any medium, provided the original work is properly cited.